CHARACTERIZATION OF METAL NANOPARTICLE INTERACTIONS WITH SMALL MOLECULES

by

Brandi J West

A thesis submitted to the Department of Chemistry

in conformity with the requirements for

the degree of Masters of Science

Queen's University

Kingston, Ontario, Canada

(June, 2009)

Abstract

The interaction between metal nanoparticles and small molecules has been investigated by FTIR and UV-visible absorption spectroscopy. Electrospray deposition into an argon matrix was chosen as the initial method. An electrospray metal source was tested in development stage. Both the formation of a stable corona discharge as well as a stable Taylor cone were successfully completed. Problems arose when the entire system was tested. It was determined that the vacuum was insufficient for the length of the flight path. Focus then shifted to nanoparticles in more conventional environments. Sol-gel encapsulated nanoparticles were generated, in the form of both monoliths as well as thin film coatings on silicon wafers. The gels were exposed to 1atm of carbon monoxide in a gas cell. The method encountered problems due to spectral interference from the matrix. The next attempt consisted of solution stabilized nanoparticles. The solution was exposed to various amounts of both ammonium sulphate and diethylamine. There was again the problem of solvent interference, even when attempting to observe the system using Raman spectroscopy. Finally, surface stabilized nanoparticles were generated, using 3-mercaptopropyltrimethoxysilane to adhere the particles to glass slides. While the coating was successfully applied to the glass slides, as confirmed with Raman spectroscopy, it was not possible to get the nanoparticles to adhere. Future outlook for this project is briefly reviewed.

Acknowledgements

I would like to take this opportunity to thank everyone who has helped me through the last three years. Some have helped me directly with the project while others have helped me through their support and pleasant distractions when things became too much to handle.

I would first like to offer my most sincere thanks to my supervisor, Prof. Dr. Mark Parnis, without whom I can safely say I would not have succeeded. His support and guidance was invaluable, and he gave me the confidence to push forward through all the difficulties faced in this project, and I know that I am all the better because of it. I would also like to thank Dr. Andrew Vreugdenhil who lent me his vast knowledge throughout this work.

I would like to extend my gratitude to all my friends and colleagues at both Queen's and Trent University. They have helped me in many ways, from allowing me to talk about my work and possible glean a new insight through our conversations, to convincing me of the necessities to go out and enjoy some free time with them. I can't express how valuable those times were, which reminded me that work wasn't everything.

Most importantly, I want to thank my family. Without them I know that I would have never made it this far. They have celebrated with me when things have gone well, and comforted me when they were going poorly. Their constant encouragement and support has given me the strength to continue forward, and to finish what has been the most frustrating, and most rewarding of endeavours.

So from the bottom of my heart, I would like to thank you all. It's been a long road but it's finally done, and I'm so grateful that you have all stuck by me. It has been rough but it was worth it.

Table of Contents

List of Figures

List of Tables

List of Abbreviations

ATR	Attenuated Total Reflectance
DEA	Diethylamine
ESI	Electrospray Ionization
FTIR	Fourier Transform Infrared Spectroscopy
GPTMS	3-glycidoxypropyltrimethoxysilane
GT gel	GPTMS-TMOS gel
HOMO	Highest Occupied Molecular Orbital
HSAB	Hard and Soft Acids and Bases Theory
IR	Infrared
LSPR	Localized Surface Plasmon Resonance
LUMO	Lowest Unoccupied Molecular Orbital
MPTMS	3-mercaptopropyltrimethoxysilane
NPs	Nanoparticles
RGA	Residual Gas Analyzer
$SC_{10}SO_3$	Sodium-1-decyl-sulfonate
SDS	Sodium dodecylsulfate
SERS	Surface Enhanced Raman Spectroscopy
SPR	Surface Plasmon Resonance
STEM	Scanning Transmission Electron Microscopy
TEM	Transmission Electron Microscopy
TEOS	Triethoxysilane
TMOS	Trimethoxysilane
UV/vis	Ultraviolet and Visible Spectroscopy

Chapter 1

Introduction

Metals have been used for some time as catalysts for various reactions including oxidation. The reacting species are adsorbed onto the metal surface where the reaction takes place.[1] The best heterogeneous catalysts are those with a large surface area; this makes metal nanoparticles ideal for this application. Their small size gives them a much larger surface to volume ratio relative to their bulk metal counterparts. This small size, which falls on the same size scale as the wavelength of ultraviolet and visible light photons, also allows the particles to interact with the photons through their delocalized electrons.

Metal nanoparticles can be used the same way as bulk metal catalysts, where they exist as a support for the reagents. Palladium-coated gold nanoparticles can be used, with hydrogen acting as a reducing agent, in the dehalogenation of tetrachloroethene.[2] No photochemical processes were employed; the nanoparticles were behaving as a metal catalyst. It was shown that palladium-coated particles could be used in this way as a very effective catalyst for this reaction, with 99% dehalogenation after one hour.

When a photon interacts with the particle it causes the electrons to oscillate around the particle which creates a localized increase in the electromagnetic field.[3] This is known as a localized surface plasmon. This plasmon allows the nanoparticles to participate in photochemical processes, by transferring electrons to the adsorbed species. Another way to use metal nanoparticles in photochemical process is through the attachment of photoactive molecules to their surface. The binding of fluorophores to metal surfaces often result in the quenching of excited states through energy transfer and electron transfer to the metal particle. The particle can then store the charge for other reactions.[4] The reverse can also be true, and the emission of the fluorophore can be enhanced if the nanoparticle is already charged through other methods.[4]

Catalytically, these various pathways allow metal nanoparticles to enhance photodissocation. An example is the photochemistry of I_2 on rough metal surfaces. A. Nitzan and L. E. Brus showed an enhancement of the absorption cross section of I_2 when in proximity to silver, gold and copper spheres.[5] This increase in absorption is further increased the closer the molecules are to the surface.

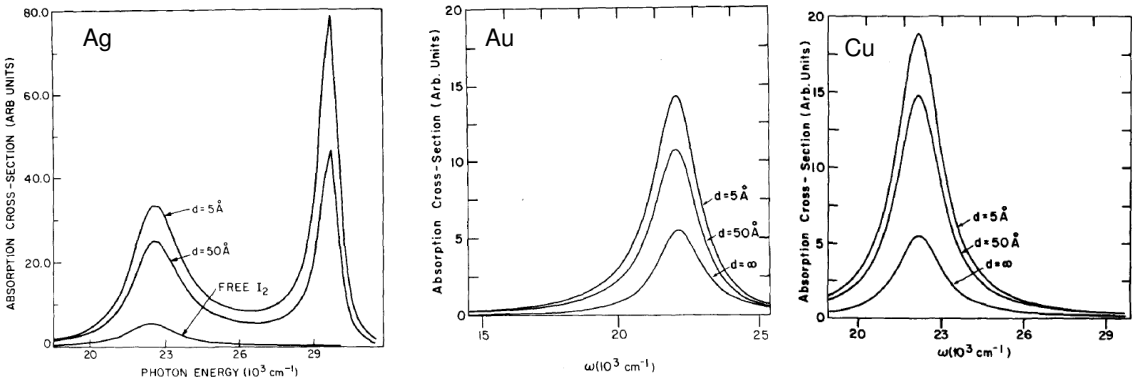

Figure 1: Absorption cross section of I_2 in proximity to metal nanoparticles.[5]

Due to their lack of stability out of solution, most reactions involving metal nanoparticles are conducted in aqueous solutions. In this work, the aim is to remove the particles from their aqueous state and attempt to characterize their interactions with small molecules. Various methods have been chosen based on their success in maintaining the stability of metal nanoparticles for other purposes. The methods employed are; electrospray ionization, sol-gel encapsulation, surface treatment. The interactions were also investigated in aqueous solution, to remove any influence of the conditions present in the other techniques.

In this project, the interactions between metal nanoparticles and small molecules were investigated using various methods. The overall goal was to characterize these interactions and to investigate any potential photochemical processes which might be useful in the field of heterogeneous catalysis. The small molecules initially chosen were gas phase molecules; therefore it was necessary to introduce metal nanoparticles into the gas phase as well. An

electrospray ionization source was produced and investigated as a method to achieve this end. Sol-gel encapsulation was another method tested for the interface with the gas phase. When the focus shifted to solution phase sample molecules, the methods used were direct observation in the solution phase as well as surface support. Surface support was a method chosen in an attempt to increase the concentration of the metal nanoparticles in order to increase the number of observed interactions.

1.1 Techniques

1.1.1 Electrospray Ionization

In the field of mass spectrometry, it is often necessary to introduce a non volatile species into the gas phase. One of the ways to achieve this is through electrospray ionization.[6] Electrospray ionization is described as a soft ionization technique which facilitates this transition from solution to gas phase, and is extremely useful for large, non volatile, chargeable molecules.[7]

The electrospray source can be considered to consist of at least three distinct regions; the first is held at atmospheric pressure where the droplets are formed, the second at slightly reduced pressure where the ions are formed, and the last region is at the lowest pressure where the target for the ions is found, be it the mass spectrometer or the stage where they will be deposited.

In the first section, the droplets are formed by forcing a solution, typically polar in nature, through a capillary held at high electrostatic potential. At the tip of the capillary the electric field produced is typically 10^6 Vm^{-1} which is high enough to cause a charge separation in the solution, with the like charged species accumulating at the tip.[7]

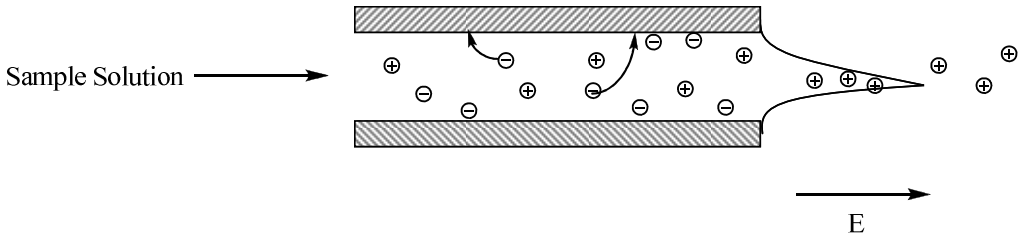

Figure 2: Schematic of capillary in a typical electrospray source.[7]

When the build up of charge at the tip of the capillary outstrips the surface tension of the solution, a Taylor cone is formed, where the solution is drawn downfield, away from the capillary.[8] This produces a spray of charged droplets of various sizes which will be reduced, through fission of the droplets and evaporation, to ions.

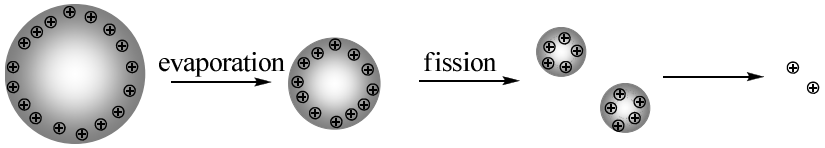

Figure 3: Diagram demonstrating the methods of reducing charged droplets to ions.

Just past the capillary tip, there is typically a jet of counter propagating gas which is what allows for evaporation of the solvent. As the solvent evaporates, the droplet is reduced in size, though the amount of charge remains the same. Once the magnitude of the charge overwhelms the surface tension of the droplet, known as the Rayleigh limit, the droplet will undergo fission, or coulomb explosion.[8] This process is repeated until only the charged molecule remains.

A similar technique to electrospray ionization is atmospheric pressure chemical ionization. The main difference is instead of a capillary under high voltage, the solution is introduced as a neutral spray from a nebulizer. The ions are formed from molecule ion interactions in the atmospheric pressure region before travelling to the target. These ions are produced from a corona discharge of a counter propagating gas. For this reason, an electrospray source and an APCI source can be interchanged readily.[7]

A corona discharge is a phenomenon which occurs when a high potential is applied, in this case to a small needle. When the potential is sufficiently concentrated, electrons can be stripped from gas molecules, which leaves them ionized. A glow can be observed as free electrons are recombined with the ionized gas.[9] This allows for chemical ionization reactions to occur between the ionized gas and the neutral sample spray.[10]

Following the formation of the ions, there is a region of both a potential gradient as well as a pressure gradient. This serves two purposes: the first is to reduce the pressure to that which a mass analyser can tolerate, while the second is to direct the ions towards the analyser. The pressure gradient is achieved through subsequent regions of vacuum pumping, as well as the use of skimmer cones which limit the number of particles which can get from one area to the next. The potential gradient uses charged plates to direct the ions towards the detector. These electrostatic lenses behave similarly to optical lenses, in that they can focus the beam of ions into a tight stream through the use of electrical potential.[7] This ion beam can then be directed to the target, often a mass spectrometer. Electrospray ionization also has applications in material chemistry as it has been shown to be an effective deposition technique where a high degree of control is needed, such as when the deposit is only wanted on parts of the surface.[11]

1.1.2 Fourier Transform Infrared Spectroscopy

All molecules have the ability to interact with light of various wavelengths. In the case of infrared spectroscopy, this interaction is in the form of the coupling of light in the infrared wavelength region with the quantized molecular vibration motions.[12] There are two common forms of spectroscopy which utilise infrared radiation, Fourier transform infrared spectroscopy (FTIR) and Raman spectroscopy.

When a molecule is irradiated with radiation of the correct frequency, a vibrational transition can be stimulated with the adsorption of the photon which causes the molecule to

vibrate more vigorously.[13] In order for a molecular vibration to be considered infrared active, this vibration needs to induce a change to the dipole moment.[12]

1.1.2.1 Transmission FTIR Spectrometer

The first component of an FT infrared spectrometer is the infrared source. The radiation needed can be supplied fairly easily using a ceramic heater, either a conducting wire coated in ceramic or a conducting ceramic source. Ceramic is chosen due to its ability to emit stable infrared radiation, and its long lifespan at these temperatures.[14]

Following the source, the next component is the interferometer. An interferometer consists of a 50% transmission mirror which allows half the light to pass straight through while the other half of the light is reflected. This mirror is positioned at a 45° angle. The two flat mirrors are positioned so that one mirror which is at a fixed position is perpendicular to a second mirror which is able to move, these mirrors are on either side of the beam splitter so that each receive 50% of the radiation. The moveable mirror moves through a range of different positions so that when the light is reflected back at the beam splitter, they will be out of phase to an extent that depends on the difference in distances between the two mirrors.[10]

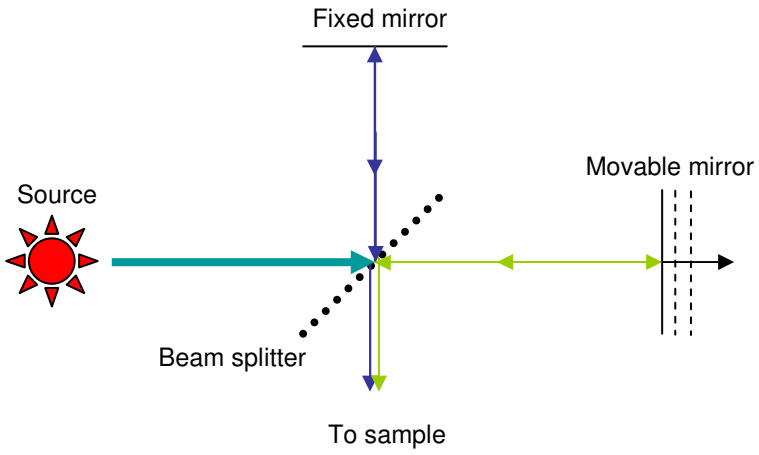

Figure 4: Schematic of Michelson interferometer.

When both mirrors are equidistant from the beam splitter, the light reflected from both mirrors is perfectly in phase and the intensity is at a maximum. When the mirror is moved from this position the intensity fluctuates in a predictable manner.[15] If monochromatic light is used, this results in a cosine wave. In the case of white light, an interferogram similar to that shown in figure 5 is produced.

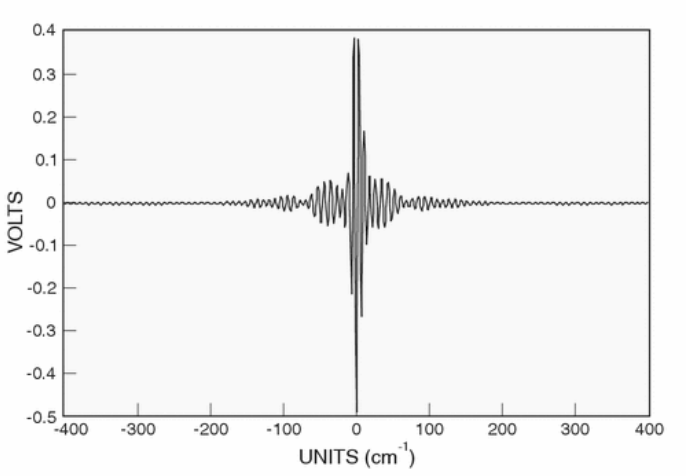

Figure 5: Broadband source interferogram.[16]

The light then travels through the sample where some of it will be absorbed based on the vibrational frequencies of the sample molecule.

The final component of the infrared spectrometer is the detector. It creates an interferogram based on the amount of radiation remaining. Using Fourier transforms, this interferogram can be converted into a frequency-domain spectrum.[14] For each spectrum collected, a background spectrum is taken. This background is to account for the intensity of the source at each wavelength, and the losses in the instrument.[14] Typically, for each experiment two spectra are produced, a reference spectrum as well as the sample spectrum. The reference spectrum contains everything that would be present in the sample spectrum except the sample itself; such as the solvent, the cell used, and any other known impurities which would be present. The purpose of this is so that the features in the sample spectrum which are associated with these

species can be identified and disregarded so that the spectrum of the sample can be accurately determined.

1.1.2.2 ATR IR Spectrometer

In some cases, transmission spectroscopy isn't an option due to the nature of the sample, such as an aqueous solution where the solvent would absorb too much of the radiation and obscure the spectrum. In these cases, attenuated total reflectance (ATR) spectroscopy is employed. This method employs the concept of internal reflectance to obtain a spectrum. Total internal reflectance occurs when the incident light passes through a medium of a certain refractive index, $n_{crystal}$, at a specific angle, know as the critical angle. If a different medium with a lower refractive index, n_{sample}, is in direct contact with the first medium, then the light can enter into it slightly before it is reflected. If the angle of the light exceeds the critical angle, θ_i; this radiation is knows as the evanescent wave.[10]

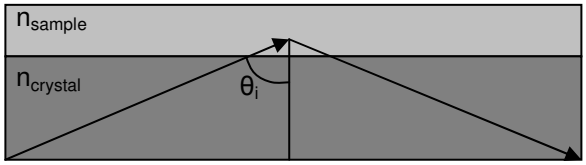

Figure 6: Graphical representation of total reflectance with evanescent wave.

For single bounce ATR, this process is only done the once before the remaining radiation is sent to the detector; in standard ATR spectrometers this is done several times before reaching the detector.

When the evanescent wave penetrates the sample, some of the light can be absorbed as with the transmission FTIR. This absorption of radiation yields the same spectrum as the transmission spectrometer with the exception of peak intensities.[15] This allows for the circumvention of solvent interference as the radiation doesn't need to pass through the entire

sample. The evanescent wave can penetrate the sample from as little as a fraction of a wavelength to as large as several wavelengths, depending on the incident angle.[15]

1.1.2.3 IR Spectrum

As stated, when a photon of the correct wavelength interacts with a molecule, a specific vibrational mode will be stimulated; this stimulation causes an increase in the intensity of the vibration. There are various factors which influence this interaction, mass of the atoms involved, bond strength, and the molecular environment.[17]

The mass effect is quite evident when one of the atoms involved is kept constant, such as the case of X-H bonds; when the change in the mass of X is small, there is a minute increase in stretching frequency. However, when going down the periodic table, thus getting much heavier, the frequencies are much smaller for the heavier atoms.[18] The same trend can be seen with bending frequencies.

Approximate Infrared Stretching Frequencies				
B-H 2400 cm^{-1}	C-H 3000 cm^{-1}	N-H 3400 cm^{-1}	O-H 3600 cm^{-1}	F-H 4000 cm^{-1}
Al-H 1750 cm^{-1}	Si-H 2150 cm^{-1}	P-H 2350 cm^{-1}	S-H 2570 cm^{-1}	Cl-H 2890 cm^{-1}
	Ge-H 2070 cm^{-1}	As-H 2150 cm^{-1}	Se-H 2300 cm^{-1}	Br-H 2650 cm^{-1}

Table 1: Approximate stretching frequencies of X-H bonds.

The substitution of deuterium for hydrogen is also a good example of the mass effect. A typical O-H bond has a stretching frequency of 3600 cm^{-1}; however the frequency for an O-D bond is only 2600 cm^{-1}. The change is so drastic because the mass of deuterium is twice that of hydrogen; no other atomic substitution has a change in mass this dramatic.[18]

Bond strength is another factor which affects the frequency of the vibration, the stronger the bond, the higher the frequency of the vibration. This trend can be seen when comparing the stretching frequencies of carbon nitrogen bonds. The C-N bond has a stretching frequency of approximately 1100 cm^{-1}, C=N appears at 1600 cm^{-1}, while C≡N has a stretching frequency of 2200 cm^{-1}.[1]

The last factor which affects the peak position for a particular vibrational motion is that of the molecular environment. If one were to compare the frequency of the O-H bond of an alcohol, ~3400 cm^{-1}, to that of a carboxylic acid, ~2900 cm^{-1}, this effect is apparent.[1] It doesn't necessarily have to be different atoms present, as conformational isomers show a similar trend. Looking at the out of plane bending frequency of the C-H bond in a cis versus trans conformation there is a visible difference in the peak locations. The cis conformation has a peak at 700 cm^{-1} while the trans conformation appears at 970 cm^{-1}. All these different criteria allow for the easy discrimination between very similar molecules as every FTIR spectrum is unique, even those which have the same molecular formula.[19]

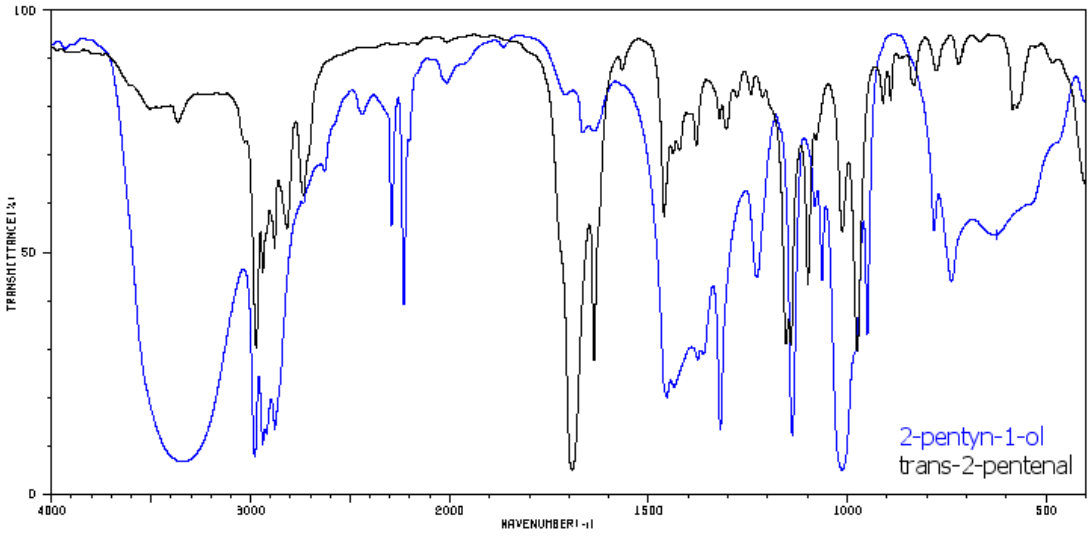

Figure 7: Comparison of infrared spectra of constitutional isomers of C_5H_8O.

The spectrum becomes more complicated when the samples are in the gas phase. This is due to the presence of distinct rotational modes which are excited simultaneously with the vibrational modes. This property has the effect of splitting the single feature of the vibrational mode into several lines with an exact separation based on the rotational constant of the molecule.[12] The vibrational-rotational absorbance is always centered on either a central vibrational peak, known as the q branch, or a gap. The q branch is a pure vibrational feature.

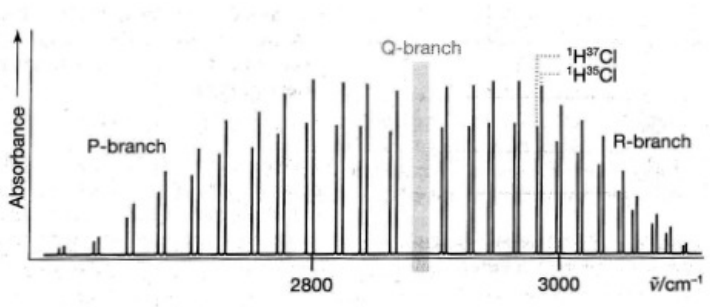

Figure 8: Typical spectrum of HCl gas with all branches labelled. In this case, the q branch is a gap.[20]

The feature associated with the q branch does not occur at the same wavenumber as the equivalent feature in the liquid phase as both molecules are in different environments. The liquid sample is perturbed, while the gas sample can be considered isolated.[21]

1.1.3 Raman Spectroscopy

Raman spectroscopy is another infrared technique, somewhat similar to FTIR spectroscopy; it's a complimentary technique which uses Raman scattering as a basis for a vibrational spectrum.[15] Raman spectroscopy occurs when light is scattered by a molecule. Light can be considered as a stream of photons, therefore light scattering can be viewed as the result of interactions or collisions between the photons and the target molecules.[22] Most scattering is elastic scattering, or Rayleigh scattering, where a photon identical to the original is liberated. This type of scattering is not useful as it gives no vibrational information about the molecule. A small

percentage is non-elastically scattered, known as Raman scattering, where the new photon is different in energy.[23]

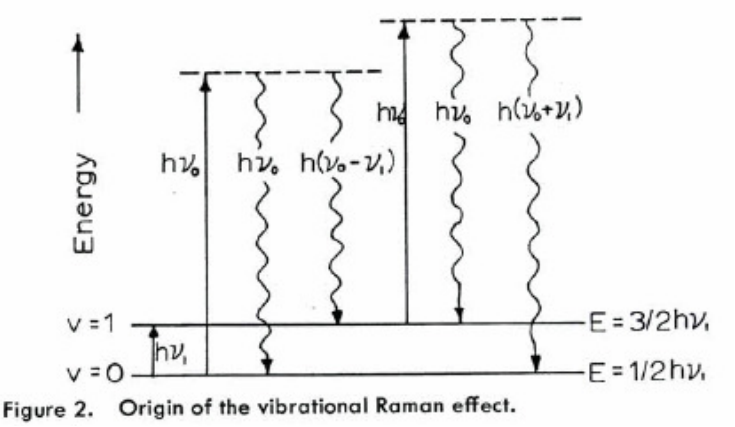

Figure 2. Origin of the vibrational Raman effect.

Figure 9: Energy level diagram demonstrating the various Raman transitions.[22]

There are two types of Raman scattering, Stokes and anti-Stokes. Stokes scattering is when the molecule is promoted to a higher vibrational energy, thus the new photon is lower in energy than the original. Anti-Stokes is the opposite, where an already excited molecule is impacted by a photon and gives the new photon more energy as it relaxes back to its ground state. This difference in energy, or frequency, of the photon is equivalent to the vibrational energy of the molecule; this is known as Raman scattering.[24] This energy is typically in the infrared spectrum and is measured in terms of Raman shift (cm^{-1}).

While FTIR relies on a change in the dipole moment of a vibrational mode in order for it to be observable, Raman spectroscopy required a change in the polarization of the molecule. Polarizability is defined as the degree of distortion in the electronic structure of the molecule caused by a given electric field.[12] Due to the different selection rules, these methods are very complementary as between both methods most vibrational modes are visible.[25]

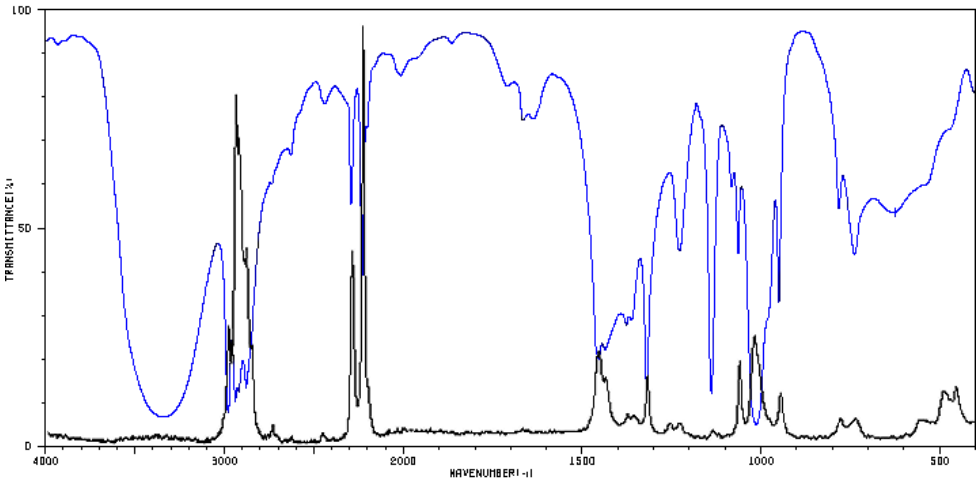

Figure 10: Spectrum of 2-pentyn-1-ol using FTIR (blue) and Raman (black).

Raman spectroscopy has many advantages as well as disadvantages when compared to infrared spectroscopy. One of the most significant advantages is in the case of aqueous solutions. Water is a large infrared absorber with intense broad features which can entirely obfuscate the spectrum of the dilute sample being investigated. In a Raman spectrum, water is practically invisible due to its low polarizability. This allows for the observation of molecules whose features are typically obscured in aqueous solution.[25] For the same reason glass can be used to contain the sample as it is also transparent to Raman scattering.

The primary disadvantage to this technique is the presence of source-induced fluorescence. Both fluorescence and Raman spectroscopy are conducted in the same manner, the resulting radiation being the only difference. As fluorescence signals can be much larger than Raman scattering this can cause problems collecting a Raman spectrum.[26] This breadth stems from the longer lifetime of a fluorescence signal when compared to the relative short lived light scattering used for Raman spectroscopy.

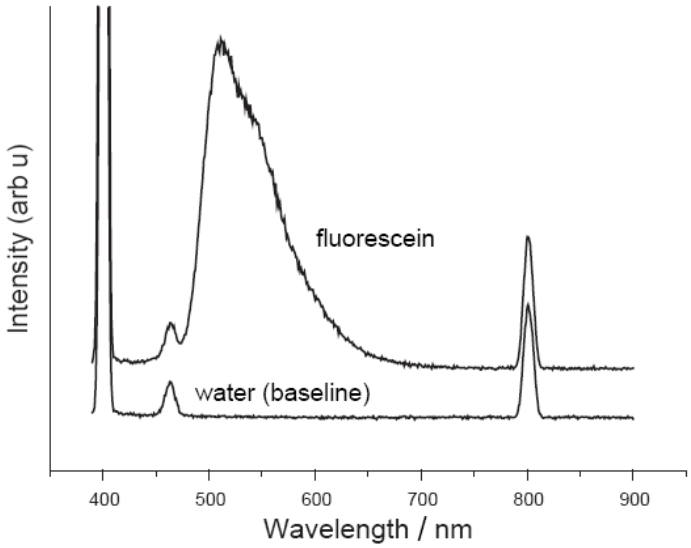

Figure 11: Comparison of fluorescence (511 nm) and Raman (462 nm) features of a fluorescein sample in water. The features at 400 and 800 nm are due to Rayleigh scattering.[26]

It is possible to reduce the influence of the fluorescence in a Raman spectrum by changing the frequency of the incident light. The fluorescent features will always occur at the same wavelength while the Raman scattering will shift according to the new frequency.[26] The broader the fluorescence peak, the less effective this solution is.

1.1.4 Metal Nanoparticles

Metal nanoparticles consist of small particles composed of one or more types of metals whose size in is the range of 1-50 nm.[27] They have been of much interest in the field of catalysis due to their unique electronic properties.[4] While nanomaterials is a fairly new field, the particles themselves have been used for various purposes for centuries. Metal nanoparticles were first recorded as being used for aesthetic purposes; their first known use was for colouring stained glass windows in the 17th century.[28] The first true scientific experiments conducted on metal nanoparticles are purported to be those of Michael Faraday in the mid 19th century. He prepared

solutions of colloidal gold through the reduction of chloroaurate $[AuCl_4]^-$ using phosphorus as a reducing agent.[29]

1.1.5 Synthetic Techniques

There are several different methods of synthesizing nanoparticles, all of which fall under one of two categories. The first category consists of starting with the bulk material and reducing the size until it is on the nanoscale, such is the case with laser ablation. The second category, which was used for this work, is the bottom-up method which consists of starting with metal atoms and building nanoparticles from them.[30] An example of this type of synthesis is the reduction of metal salts.

One of the most widely used methods of nanoparticles synthesis is the reduction of metal salts.[29] This method allows for the formation of not only mono-metallic particles but also bimetallic and polymetallic particles. It is a typical redox reaction which has the following general formula,

$$m\mathrm{Me}^{n+} + m n\mathrm{Red} \rightarrow m\mathrm{Me}^{0} + m n\mathrm{Ox} \qquad (1)$$

where Me signifies the metal species, and Red/Ox represents the reducing – oxidizing pair. The redox potential of the half cell reactions determines the effectiveness of the reaction. Because of this, the more electropositive metals can react with a wide range of reducing agents, even if they aren't very electronegative.[31]

In all cases, this method consists of introducing a metal salt of the desired metal, as well as a suitable reducing agent into solution with, in certain cases, appropriate stabilizing agents. In some instances the reducing agent can function as both a stabilizer and reducer, such as sodium citrate. When non-polar solvents are used, the reducing agent and the solvent can occasionally be one and the same.[29] Water, however, is the most commonly used solvent as it is inexpensive, readily available and not harmful.

Depending on the stability of the metal chosen, stabilizing agents are sometimes required. There are two types of stabilizing methods: electrostatic stabilization and steric stabilization. Electrostatic stabilization uses the counterions present in the solution to repel the particles from each other so that they do not agglomerate. The reducing agent can often behave as an electrostatic stabilizer, as is the case of sodium citrate; the excess forms an electric double layer around the particles. The electrostatic repulsion of these layers are stronger than the van der Waals forces drawing the particles together.[29] Steric stabilization uses bulky surfactant molecules to physically force the particles apart strictly due to their size.[27] Sodium dodecylsulfate is an example of a commonly used steric stabilizer; the sulfate adsorbs onto the particle surface and the long carbon tail prevents other particles from getting close enough to agglomerate.

There are different types of polymetallic nanoparticles, such as core shell particles as well as homogenously distributed particles. In the case of core-shell particles, a second metal salt is either introduced into the solution after the core particles have already been formed, or is significantly less electropositive than the core metal. This allows for a shell of the second metal to form around the first. This method is desirable when the secondary metal has useful chemical properties but on its own the metal is unstable in the nanoscale. If the two metals used are relatively equally electropositive and are added simultaneously a homogenous mixture of the two is possible.[31]

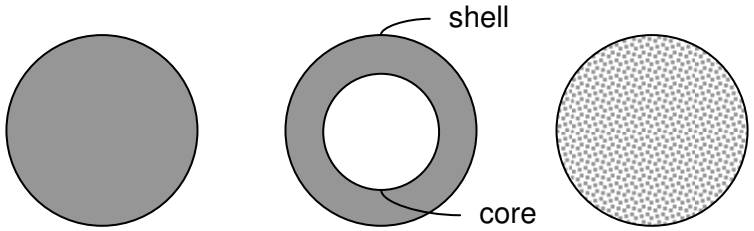

Figure 12: Schematic of a monometallic nanoparticle compared to core-shell and homogeneous bimetallic particles.

1.1.6 Catalysis

Metals are often used as heterogeneous catalysts for some reactions; primarily hydrogenation and dehalogenation. This is due to the ease with which the catalyst can be removed from the final product and can be reused.[1] The reaction occurs on the metal surface; the reagents are adsorbed and react before they are subsequently desorbed.[12]

For heterogeneous catalysis, surface area is one of the more important properties of the catalyst. This makes nanoparticles prime candidates due to their high surface area to volume ratio. Nanoparticles also have the added advantage of being able to participate in photocatalysis due to surface plasmon excitation.[4]

Due to their size, on the same scale as the wavelengths of visible or ultraviolet light, nanoparticles have two different ways to participate in photochemical processes. When the photon's wavelength is the same as that of the surface plasmon, some of the nanoparticle's electrons can be transferred to the adsorbed species through its plasmon resonance. In the case when the photon's energy is not that of the surface plasmon, then the nanoparticle can still absorb the energy if the surface of the particle has been treated with fluorophores or dyes.[4]

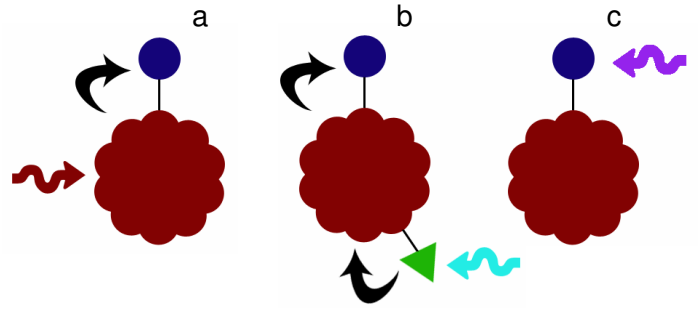

Figure 13: Schematic of photochemical processes involving metal nanoparticles. a) Nanoparticle is excited and transfers energy to adsorbed molecule. b) Adsorbed dye molecule is excited and energy is transferred to adsorbed molecule through nanoparticle. c) Adsorbed molecule is excited directly.

One of the primary uses of metal nanoparticles which take advantage of their photochemical properties is that of surface enhanced Raman spectroscopy (SERS). The molecule of interest is adsorbed onto the metal nanoparticles, either silver or gold. The resulting scattering is significantly enhanced, between 10^3-10^6 times greater than in solution. There are two factors which contribute to this increase in signal, an increase in the electromagnetic field, and the formation of a charge transfer complex.[23] The laser light used for Raman spectroscopy is usually close in wavelength to that of the localized surface plasmon of gold or silver metal nanoparticles. When the incident light is of the same frequency as the metal plasmon, the particles enhance the intensity of the electromagnetic field at the metal surface.[3] This increase in the local electromagnetic field increases the vibrational modes which are perpendicular to the metal surface.[23] Certain molecules showed an even greater enhancement that what can be explained by the electromagnetic factor. Molecules which possess lone pair electron or pi clouds can be chemisorbed onto the metal surface. If the Fermi level of the metal lies at energy symmetrically between the HOMO and the LUMO of the adsorbed species, the visible light from the Raman source is of sufficient energy to make up the difference. The metal species acts as an intermediate and the photon only needs to have half the energy normally needed for the transition, to go from the Fermi level of the metal to the LUMO of the adsorbed molecule.[32]

1.1.7 Surface Plasmon Resonance Spectroscopy

Metal nanoparticles have the distinct ability of being able to resonate with light in the form of the production of a localized surface plasmon. A plasmon refers to the quantized oscillation which occurs in species which have delocalized electrons, as is the case with metals, when these electrons are disturbed from their equilibrium state.[33] In the case of surface plasmons, this phenomenon occurs on the metal surface. Surface plasmons have significantly lower

frequencies then their bulk counterparts.[33] This allows them to be excited by ultraviolet and visible light under certain conditions.

Metal particles exhibit localized surface plasmons which, unlike propagating surface plasmons, consist of a static wave. A surface plasmon is the result of the motion of all the free electrons of a particle toward one side.

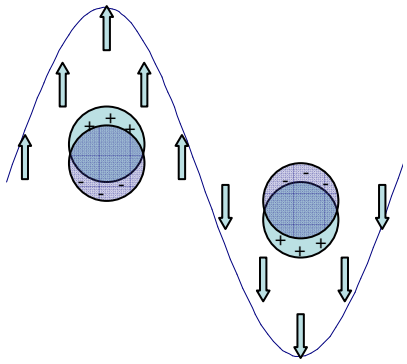

Figure 14: Graphical representation of a localized surface plasmon.

When a wave of incident light of the correct wavelength interacts with a metal particle, the electric field induces a sort of dipole within the particle. A negative pole due to the electron cloud being repelled from the wave, and a positive pole centered on the particle due to the metal nuclei. For this phenomenon to occur, the particle must be smaller than the wavelength of light.[34] The specific wavelength of light which causes this occurrence depends on not only the type of metal but also the size and shape of the particle, as well as the refractive index of the medium in which it is occurring.[35]

In the case of spherical nanoparticles this interaction is well described using Mie theory. Mie theory is a solution to the Maxwell equation which describes the interactions between a plane wave and a homogeneous sphere.[36]

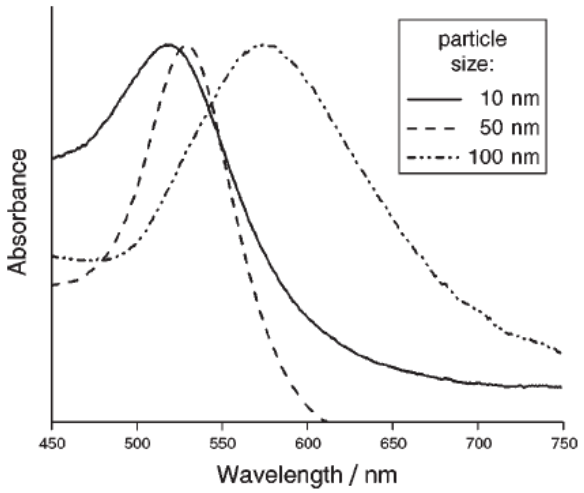

Figure 15: SPR spectra of 10, 50 and 100 nm Au particles. [33]

Particles of the same composition but of different sizes experience a shift in their plasmon peak with the shift occurring in the red direction with increasing particle size. For spherical nanoparticles, only one plasmon peak is evident as all dimensions of the particle are equal. For non-spherical particles, this is no longer true and they can therefore have multiple features in their spectrum.[37] In the case of nanorods the longer axis, the longitudinal axis, has the plasmon with the lower energy.[33] The more complex the shape of the particle the more features the extinction spectrum would contain.

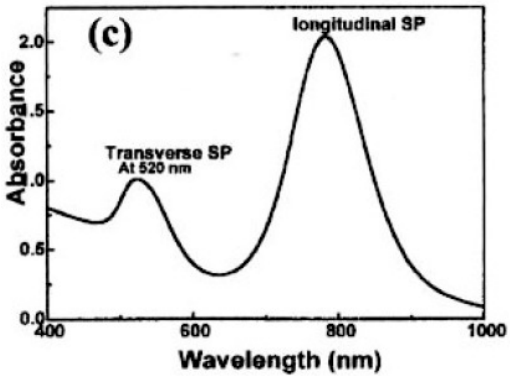

Figure 16: LSPR spectrum of gold nanorods.[37]

The environment of the particle also has a significant effect on the extinction spectrum; there are two main environmental influences, the solvent used as well as ligands which may interact with the particles directly.

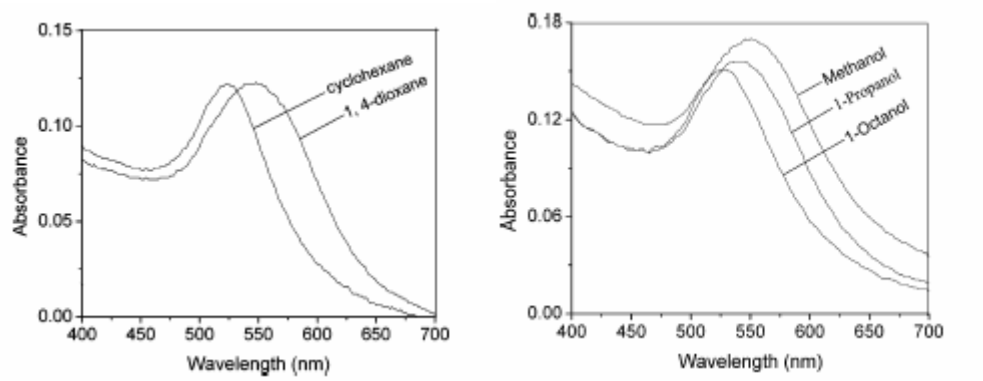

Figure 17: a) Surface plasmon adsorption band of gold nanoparticles in cyclohexane and 1,4-dioxane. b) Surface plasmon adsorption band of gold nanoparticles in methanol, 1-propanol and 1-octanol.[35]

It was found that in the case of solvent influence, two trends were evident. The first trend was that the peak would suffer a red shift with increasing refractive index when in inert, non-polar solvents.[35] There is a linear relationship between the wavelength of the surface plasmon and the refractive index, even when the nanoparticle itself is shielded due to its stabilizing agent.[35] The second trend revolves around solvents which were polar in nature, or have functional groups with which the particles can interact. This trend shows a non-linear relationship which behaves more in accordance with Mie theory, as the functional groups can remove electrons from the surface of the colloidal particles which would produce a noticeable shift in the surface plasmon.

The chain length of the solvent also has an effect on the surface plasmon. As, seen in figure 17, there is a minor blue shift with each additional carbon. It is believed that the shorter carbon chains allow the solvent to interact more readily with the particles, which promotes diffusion through the stabilizing layer surrounding the particle.[35]

Ligand chain length also affects the plasmon as well as functional groups. In the case of chain length, there is a red shift with each additional carbon, as seen in figure 18a.[35]

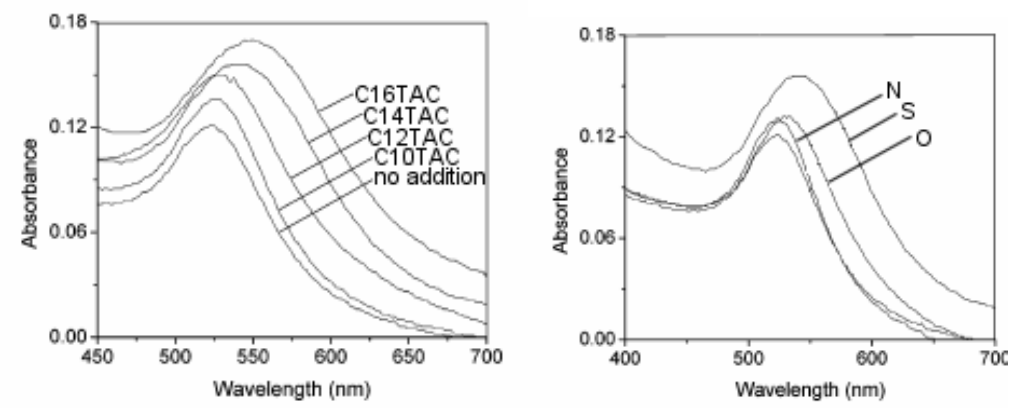

Figure 18: Absorbance spectrum of gold nanoparticles treated with a) series of cationic surfactants of increasing chainlength and b) same surfactant (1-dodecyl)with different functional groups (-NH_2, -OH, -SH).[35]

The stabilizing ligands on the surface of a particle act as a shell layer. The longer the carbon chain of this layer the larger its volume ratio becomes, which in turn increases its contribution to the dielectric function of the protecting layer. The functional head group of the ligand also has an effect on the plasmon based on the HSAB theory. The softer head groups interact and bind more strongly with the metal surface of the particles, thus affecting the surface plasmon to a greater extent. This is demonstrated in figure 18b, where 1-dodecanethiol has the largest effect, followed by the alcohol and amine equivalents.

1.1.8 Transmission Electron Microscopy

Transmission electron microscopy (TEM) has been used for the characterization of metal nanoparticles for some time.[2, 27, 38] This method allows for the determination of size and shape of the particles due to their high electron density.

The transmission electron microscope works similarly to a typical light microscope, except it uses an electron beam as its source instead of visible light.[39] Due to the nature of the

electron microscope, the entire column is maintained at high vacuum. This allows the electron beam to travel the entire column length with a minimum amount of loss due to scatter.[39]

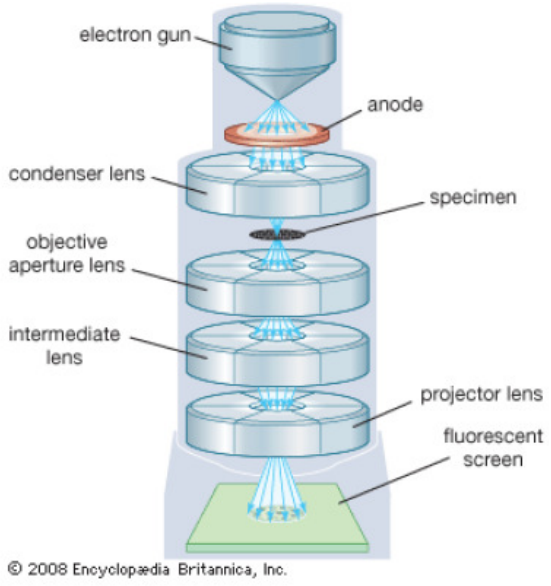

Figure 19: Schematic representation of a transmission electron microscope.

The first component of an electron microscope is the electron gun, which is the source of electrons. An electron gun typically uses thermionic emissions from a heated tungsten filament. Once the filament is heated above 2700 K, the filament begins to emit light and electrons in large quantities.[40] This filament is pointed in the middle in the direction of the electron beam. Immediately in front of the filament is an anode which acts to accelerate the electrons. There is a small hole in the center for the electrons to pass through. The beam emitted at this point is still insufficiently powerful for the purpose of electron microscopy; therefore electromagnetic lenses are used to focus the beam.[39]

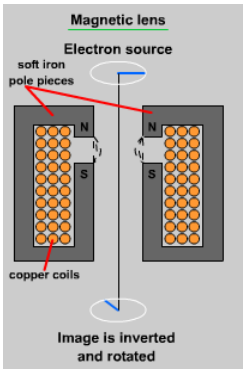

Figure 20: Graphical representation of electromagnetic lens.[41]

Electromagnetic lenses work by passing current through a coil which acts like a convex optical lens. The electric field pulls off axis rays back into focus.[41]

The next component of the microscope is the condenser lenses. Their purpose is to control the diameter of the beam so that only the sample is illuminated. The diameter required depends on the magnification of the sample, as ideally, the beam would be only slightly greater then the area of interest. This allows for the specimen observed to be as bright as possible.[40]

Following the condenser lenses is the actual sample chamber where the TEM grids are placed in a sample holder. The positioning of the sample is critical due to the small size of the sample and the high degree of magnification.[40] The sample is mounted on a metal support grid, due to the required depth of the sample. The electron beam cannot penetrate samples which are thicker than one micron, thus the TEM sample is much thinner than this.[40] To maintain the high vacuum, the sample is inserted into the column through an airlock.[39]

In the case of metal nanoparticles samples, the sample consists of a drop of the particle containing solution onto a TEM grid. This drop is then allowed to dry and the process is repeated. The amount of solution placed on the grid depends on the concentration of particles in the solution.

Below the sample chamber, there are more electromagnetic lenses which are used for the magnification and focusing of the image. The lens immediately below the sample compartment is the objective lens.[42] Its function is to improve the focus, the resolution and the contrast of the final image.[40]

The final lenses of the electron microscope are the projector lenses. These are used to produce diffraction patterns or images over the whole screen. These very strong electromagnetic lenses reduce the amount of distortion on the edges of the final image.[42]

The final component of the electron microscope is the fluorescent screen and camera. The electron beam hits the fluorescent screen and the more electrons that hit a certain area, the brighter the screen fluoresces. In the case of metal nanoparticles, due to their electron density, the image appears as black or dark grey dots or other shapes depending on the particles themselves.[39] Below the screen lies a stage which contains either a charge-coupling device camera, or photographic film. The fluorescent screen can be lifted away so that the camera or film can be exposed. From here the negative can be developed or the digital image produced.

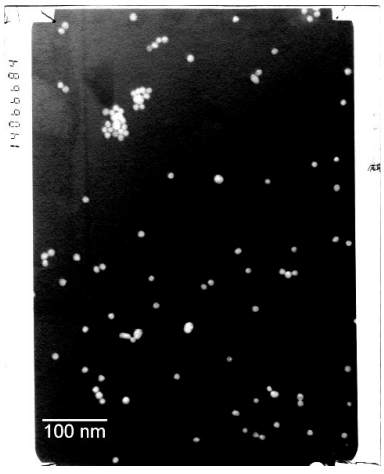

Figure 21: TEM image of gold nanoparticles produced through sodium citrate reduction.

Once the images are made, the negatives can then be scanned into a computer, or the digital images can be uploaded directly. Counting software can then be used to count and measure the diameter of the particles in order to determine a distribution of size.

1.1.9 Sol-gel Chemistry

Sol-gel materials consist of organic and inorganic polymers synthesized through the sol-gel process. This process consists of the transition of colloidal suspensions, known as sols, into viscous gels which eventually harden into brittle, porous solids.[43] The two main groups of materials used for this technique are silicates and metal oxides. The elaborate polymer network is constructed through various steps of hydrolysis and condensation.[44]

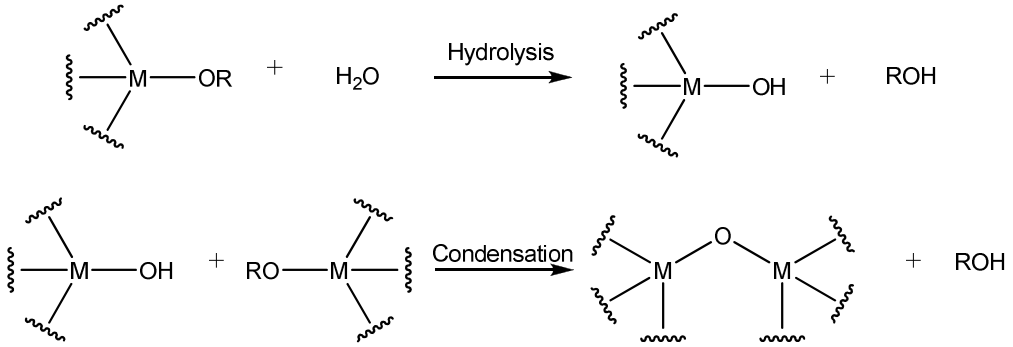

Figure 22: General reaction equation for the sol-gel processes of hydrolysis and condensation.[44]

Where M represents either a transition metal or silicon atom. This process occurs several times throughout the solution, which is called the gelation. As the solution gels it will form a skin on the surface of the solution which traps the remaining solution, allowing it to solidify as well over an extended period of time. This is where the 'crosslinking' network occurs, a complex polymerization through the solution. One of the largest advantages to sol-gels over other materials is that they can be formed in ambient conditions; they don't need excessively high temperatures or pressures.

Once the polymerization is complete, there is an excess of alcohol and water present as a by-product of the condensation reaction. These solvents occupy the empty spaces in the gel, keeping them porous. Since these solvents are volatile, their evaporation causes the gel to shrink and harden as the pores are emptied. The more solvent that is removed, the more the gel will shrink until there are no pores left.[43]

For silicate based sol-gels, the reactions are often acid or base catalyzed, depending on the type of sol-gel being made. In an acidic environment, subsequent hydrolysis reactions become increasingly difficult, whereas in base catalyzed reactions this process becomes easier. This results in the formation of more linear polymers in acidic mediums and branched clusters forming under basic conditions.[45] In the case of 'acidic' gels, the result would give a more homogeneous, dense gel with very small pore size. The more 'basic' gels, however, gel quite rapidly and yield a more porous network.[43]

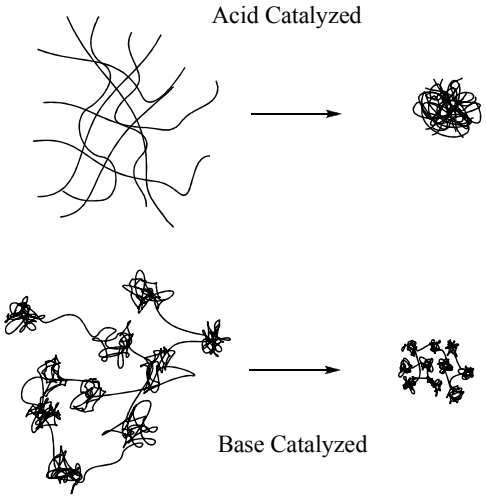

Figure 23: Comparison of finished gels under acidic and basic conditions.[43]

Due to their nature, sol-gels can be made into various types of materials. The most common of these are thin film coatings and three dimensional monoliths.

Monoliths are the most facile of the materials to make as they need only be poured into a mould while still in a liquid state and allowed to harden.[46] The primary complication with this is

that, while drying, the shrinkage of the gel will often cause minute cracks to form on the surface, and if allowed to dry out entirely, they will break apart.[43]

For thin films, there are three primary methods for application, spin-coating, dip coating and draining. All these methods allow for uniformly thin films, typically 1 μm thick, to be adhered to the entire surface of the substrate, even if it is of a complex form. Thin films do not exhibit the cracking seen in monolith structures as all the shrinkage is show to be taken up by the thin dimension and not in the plane of the substrate.[46]

There are many applications for both thin films and monoliths. Thin films are often used in the form of optical coatings. Specifically, sol-gels have been used for antireflective, half mirrors and hot or cold mirrors; this is in lieu of other application methods.[46] Sol-gels allow for homogeneous coatings of large, curved surfaces. Multiple layers of different compositions call also be employed for light filtering purposes, whereas other methods cannot achieve this.[43]

Monoliths, and to a lesser extent thin films, are used extensively for their ability for encapsulation. Due to their porosity, other species can be included in the gel and still be accessible. This allows the gel to behave like a matrix, which holds the included species in place while still allowing access to the exterior environment. Two applications which take advantage of this are in the field of chemical sensors and catalysis.[43]

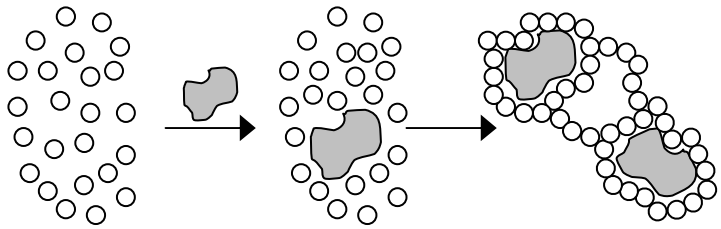

Figure 24: Schematic representation of encapsulation process in sol-gel.[43]

Sol-gels are typically transparent which allows these encapsulation properties to be exploited for optical systems as well, where the included species are chromophores.[46]

References for Chapter 1

1. Bruice PY. Organic chemistry. 4th ed. Upper Saddle River, USA: Prentice Hall; 2004.

2. Nutt MO, Heck KN, Alvarez P, Wong MS. Improved pd-on-au bimetallic nanoparticle catalysts for aqueous-phase trichloroethene hydrodechlorination. Applied Catalysis B, Environmental 2006 December 1, 2006;69(1-2):115-25.

3. Weaver GC, Norrod K. Surface-enhanced raman spectroscopy: A novel physical chemistry experiment for the undergraduate laboratory. J Chem Educ 1998 May 1998;75(5):621-4.

4. Kamat PV. Photophysical, photochemical and photocatalytic aspects of metal nanoparticles. J Phys Chem B 2002 AUG 15;106(32):7729-44.

5. Nitzan A, Brus LE. Theoretical-model for enhanced photochemistry on rough surfaces. J Chem Phys 1981;75(5):2205-14.

6. Senko MW, McLafferty FW. Mass spectrometry of macromolecules: Has its time now come? Annu Rev Biophys Biomol Struct 1994 06/01;23(1):763-85.

7. Gross JH. Mass spectrometry. 1st ed. Berlin: Springer; 2004.

8. Gaskell SJ. Electrospray: Principles and practice. J Mass Spectrom 1997 July 1997;32(7):677-88.

9. Serway RA, Beichner RJ. Physics for scientists and engineers. 5th ed. Toronto: Saunders college publishing; 2000.

10. Harris DC. Quantitative chemical analysis. 6th ed. New York, USA: W. H. Freeman and Company; 2003.

11. Lenggoro IW, Lee HM, Okuyama K. Nanoparticle assembly on patterned "plus. J Colloid Interface Sci 2006 NOV 1;303(1):124-30.

12. Atkins P. The elements of physical chemistry with applications in biology. 3rd ed. New York, USA: W. H. Freeman and Company; 2001.

13. Ebbing DD, Gammon SD. General chemistry. 7th ed. Boston, USA: Houghton Mifflin Company; 2002.

14. Taylor N. How does FTIR work? IJVS [Internet]. [revised 2004 2004;cited November 21, 2008];5(5):November 21, 2008. Available from http://www.ijvs.com/volume5/edition5/section1.html#Feature.

15. Skoog DA, Holler JA, Nieman TA. Principles of intstrumental analysis. Fifth Edition ed. Toronto, Canada: Nelson Thomson Learning; 1998.

16. Introduction to FT-IR Spectroscopy [Internet]Irvine, CA: Newport Corporation; c2009 [cited 2009 May 21]. Available from: http://www.newport.com/Introduction-to-FT-IR-Spectroscopy/405840/1033/catalog.aspx.

17. Pimentel GC. Infrared spectroscopy: A chemist's tool. J Chem Educ 1960;37:651.

18. Infrared Spectroscopy Primer: The Nature of Vibrational Spectroscopy [Internet]: John Wiley & Sons, Ltd.; c2008 [cited 2009 May 18]. Available from: http://www.spectroscopynow.com/coi/cda/detail.cda?id=18428&type=EducationFeature&chId=2&page=1.

19. Coates J. Interpretation of infrared spectra, A practical approach. In: R. A. Meyers, editor. Encyclopedia of analytical chemistry. Chichester: John Wiley & Sons Ltd; 2000.

20. Atkins P, De Paula J. Physical chemistry. 7th ed. New York: W. H. Freeman; 2002.

21. Taylor N. Infrared spectroscopies of gases. IJVS [Internet]. [revised 2004 2004;cited November 28, 2008];5(3):November 28, 2008. Available from http://www.ijvs.com/volume5/edition3/section1.html.

22. Tobias RS. Raman spectroscopy in inorganic chemistry .I. theory. J Chem Educ 1967;44(1):1.

23. Raman Tutorial [Internet]Ann Arbor Michigan: Kaiser Optical Systems, Inc.; c2009 [cited 2009 May 17]. Available from: http://www.kosi.com/Raman_Spectroscopy/rtr-ramantutorial.php?ss=800.

24. Raman [Internet]: National Research Council of Canada; c2006 [cited 2008 Dec/4]. Available from: http://ibd.nrc-cnrc.gc.ca/research/spectroscopy/2_raman_e.html.

25. Tobias RS. Raman spectroscopy in inorganic chemistry .II. applications. J Chem Educ 1967;44(2):70-6.

26. Clarke RJ, Oprysa A. Fluorescence and light scattering. J Chem Educ 2004 May 2004;81(5):705-7.

27. Bonnemann H, Richards RM. Nanoscopic metal particles - synthetic methods and potential applications. European Journal of Inorganic Chemistry 2001 OCT(10):2455-80.

28. Rao CNR, Kulkarni GU, Thomas PJ, Edwards PP. Metal nanoparticles and their assemblies. Chemical Society Reviews 2000 2000;29(1):27-35.

29. Schmid G, editor. Nanoparticles: From theory to application. 1st ed. Weinheim: Wiley-VCH Verlag GmbH & Co.; 2004.

30. Cao G. Nanostructures and nanomaterial: Synthesis, properties and applications. 1st ed. London: Imperial College Press; 2004.

31. V. Goia D, Matijević E. Preparation of monodispersed metal particles. New Journal of Chemistry 1998 1998;22(11):1203-15.

32. Lombardi JR, Birke RL, Lu T, Xu J. Charge-transfer theory of surface enhanced raman spectroscopy: Herzberg-teller contributions. J Chem Phys 1986 April 15, 1986;84(8):4174-80.

33. Campbell DJ, Xia Y. Plasmons: Why should we care? J Chem Educ 2007 JAN;84(1):91-6.

34. Willets KA, Van Duyne RP. Localized surface plasmon resonance spectroscopy and sensing. Annu Rev Phys Chem 2007 05/01;58(1):267-97.

35. Ghosh SK, Nath S, Kundu S, Esumi K, Pal T. Solvent and ligand effects on the localized surface plasmon resonance (LSPR) of gold colloids. J Phys Chem B 2004 SEP 16;108(37):13963-71.

36. Syvitski JPM, editor. Principles, methods and application of particle size analysis. Cambridge University Press; 2007.

37. Hutter E, Fendler JH. Exploitation of localized surface plasmon resonance. Adv Mater 2004 OCT 4;16(19):1685-706.

38. Schwartzberg AM, Zhang JZ. Novel optical properties and emerging applications of metal nanostructures. Journal of Physical Chemistry C 2008 JUL 17;112(28):10323-37.

39. Flegler SL, Heckman , J. W. Jr., Klomparens KL. Scanning and transmission electron microscopy: An introduction. 1st ed. New York, USA: Oxford University Press; 1993.

40. Goodhew PJ. Electron microscopy and analysis. 1st ed. London: Wykeham Publications; 1975.

41. TEM Basics - Matter [Internet]Liverpool, England: Matter, University of Liverpool; c2000 [cited 2008 November, 12]. Available from: http://www.matter.org.uk/tem/default.htm.

42. Egerton RF. Physical principles of electron microscopy: An introduction to TEM, SEM and AEM. Boston, USA: Springer Science and Business Media Inc.; 2005.

43. Wright JD, Sommerdijk, N. A. J. M. Sol-gel materials chemistry and applications. 1st ed. New York: CRC Press; 2001.

44. Livage J, Sanchez C. Sol-gel chemistry. Journal of Non-Crystalline Solids 1992;145:11-9.

45. Klein LC. Sol-gel processing of silicates. Ann Rev Mater Sci 1985;15:227-48.

46. Klein LC. Sol-gel optical materials. Ann Rev Mater Sci 1993;23:437-52.

Chapter 2
Electrospray Ionization

In order to be able to get metal nanoparticles to react within a gas phase system, a method of introduction must be determined. One such method proposed was the use of electrospray ionization, which has been employed for the deposition of metal nanoparticles.[1-3] Electrospray ionization is an effective method for the removal of solvent. It is often used for this purpose in the case of non-volatile molecules, in order to introduce them into the gas phase for spectrometric analysis, where the solvent would be an impurity. This feature makes it possible to interface an electrospray source with a matrix isolation apparatus, which requires the reagents to be in the gas phase. Matrix isolation uses the freezing of argon gas, or any other inert gas, to trap reactive species for analysis. This marrying of methods would make it possible to investigate the interactions between metal nanoparticles and small gaseous molecules and learn more about the photochemical processes which may occur.

2.1 Literature Review

Electrospray was first invented by Dr. M. J. Richardson in 1963.[4] His experiment involved spraying a fine mist of high molecular weight polystyrene onto a thin carbon film for observation using an electron microscope. Good solvents were classified as those in which the polymer chain was expanded and gave large flat disk shaped droplets, while bad solvents cause agglomeration, which occurred regardless of polymer concentration. If a solvent was sufficiently volatile, it was seen that some droplets consisted of single polymer molecules. This gave the start of electrospraying.

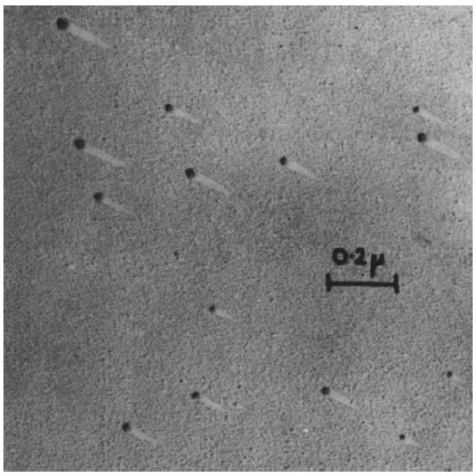

Figure 25: Polystyrene molecules sprayed from a benzene(68%)/isobutanol solution.[4]

Following this discovery, electrospray ionization was first discussed as an ionization technique for mass spectrometry by Malcolm Dole in 1968.[5] In his paper, Dole considered the various problems encountered when dealing with macromolecules for analysis, in both electrospray and non electrospray systems; which consist of droplet size, solvent evaporation and molecular aggregation.[6]

Electrospray was well suited for the analysis of macroions as it was determined that a droplet needed to be approximately 100 nm in size, to be sure that only one macromolecule was contained within each drop. Other nebulizing methods could only produce droplets between 1000- 5000 nm. The charge which allows for such small droplets to be produced also helps in the prevention of agglomeration, as it was shown that the Coulombic repulsion was often greater than the attractive forces of the polarized solvent.

He employed the use of a nozzle skimmer system which had the benefit of allowing for differential pumping, to solve the problem of spraying directly into a vacuum. If a solution were to be sprayed directly into a vacuum, the solvent would freeze before evaporating. Differential pumping solves this by having a region around the capillary at atmospheric pressure, to allow for

evaporation, before the macroions pass through to the first stage of the vacuum. A Faraday cage was used in lieu of a mass spectrometer for the analysis of the ions.

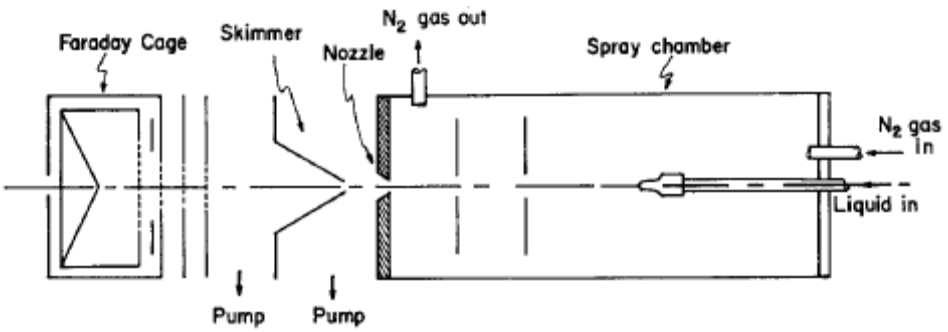

Figure 26: Schematic diagram of apparatus used by Dole.[6]

This basic design is still used for ESI with the Faraday cage replaced with which ever mass spectrometer, or other device, is to be used.

One such example is the coupling of electrospray ionization with FTIR presented by Signorell et al.[7] In this letter, the author used electrospray ionization to produce sucrose colloids of various sizes for vibrational analysis. The primary goal was to develop a method for the vibrational investigation of non volatile molecules. Electrospray proved to be an ideal means to introduce the solution to be evaluated and was successfully paired with FTIR. They were able to successfully investigate various sizes of sucrose nanoparticles and were able to determine their crystalline structure, which proved to be an amorphous solid, through comparison with bulk samples. It was also determined that for the larger particles tested, there was no evidence of size effects in their vibrational profile.

As previously stated, electrospray is also used extensively for deposition. It gives more control over the thickness and evenness of a coating. Electrostatic repulsion assures that particles are well separated, and to decrease this spacing, longer deposition times are employed.[2] Frank Schulz used electrospray coupled with pyrolysis to adhere bare nanoparticles to various surfaces.[2]

It was determined that bare metal nanoparticles, which had the citrate coating removed, adhere much more strongly to the surface when compared to those which had not.

Another property which was investigated was that of surface wetting. It was shown that depending on the size of the particles, when all other conditions were kept constant, the wettability of the surface was affected; the smaller the particles comprising the coating, the more wettable the surface.

For some applications, it becomes very important that the surface coating be as free from impurities as possible. The best way to achieve this is to form the coating under vacuum. Stephan Rauschenbach et al. were able to successfully deposit boimolecules as well as inorganic clusters onto a substrate in vacuum through the use of electrospray deposition.[3]

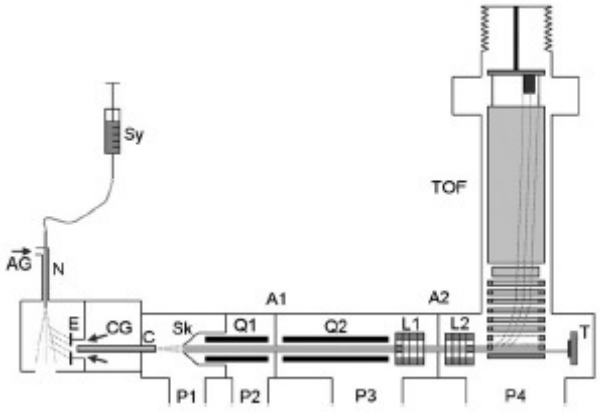

Figure 27: Schematic diagram of electrospray deposition apparatus.[3]

The design introduced the sample solution using electrospray (E), and it was then directed through the pressure gradient using quadrapole ion guides (Q1, Q2). The differential pumping was achieved using four different pumps with the pressure between each stage differing by at least an order of magnitude until in the last chamber the pressure reached 10^{-6} mbar (P4).

Organically coated gold particles were successfully deposited on highly oriented pyrolitic graphite surfaces in islands of about 250 to 640 nm wide with a height of only 3 to 17 nm. This

demonstrated to the authors that the particles did not agglomerate until they had reached the surface, if they had agglomerated in flight they would be much more spherical in nature. This led them to the conclusion that the particles were highly mobile on the surface, and that the cluster-cluster interactions were stronger than the cluster-surface ones. This high mobility of the particles was also demonstrated with the distribution of the particles on the substrate, where they preferentially decorated the step edge of the surface.

Taking the mobility of the particles one step further, Lenggoro et al. took advantage of this property, and the electrostatic behaviour of the nanoparticle ions to create a patterned deposit of nanoparticles by charging their surface.[1] A negatively charged electrified pattern was drawn on a conductive and non- or semi-conductive substrate using charge transfer. When electrosprayed, the gold particles were deposited on this pattern, a line with a width of approximately 100 nm and a length of several millimetres, with a high degree of accuracy which can be seen from the STEM image shown in figure 28.

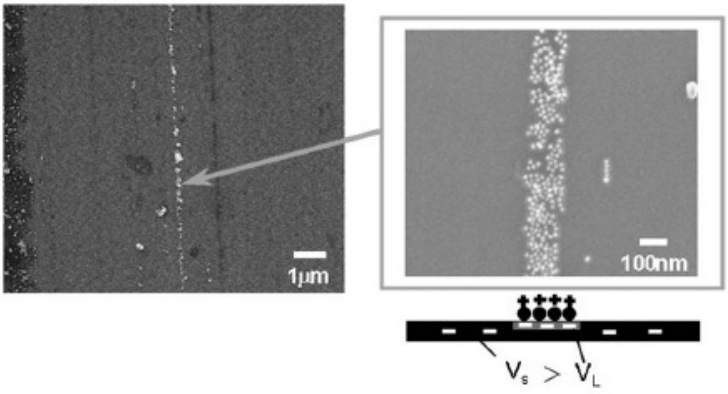

Figure 28: STEM image of 20 nm gold particles deposited on charged substrate.[1]

The information gathered from these works illustrated four key points which were applied in this project. It demonstrates that metal nanoparticles can be electrosprayed successfully for various purposes and into diverse environments. Electrospray ionization has

been successfully coupled with FTIR and can be sprayed into systems which require low pressures through the use of a pressure gradient. Finally it shows that the nanoparticles produced can be directed with a high degree of accuracy through the use of electrostatic lenses in order to transmit them over relatively long flight paths.

2.2 Experimental and troubleshooting

The electrospray apparatus used for this project is shown below. For the initial testing, each chamber was optimized separately before any attempt was made to use the entire system to spray nanoparticles at the target.

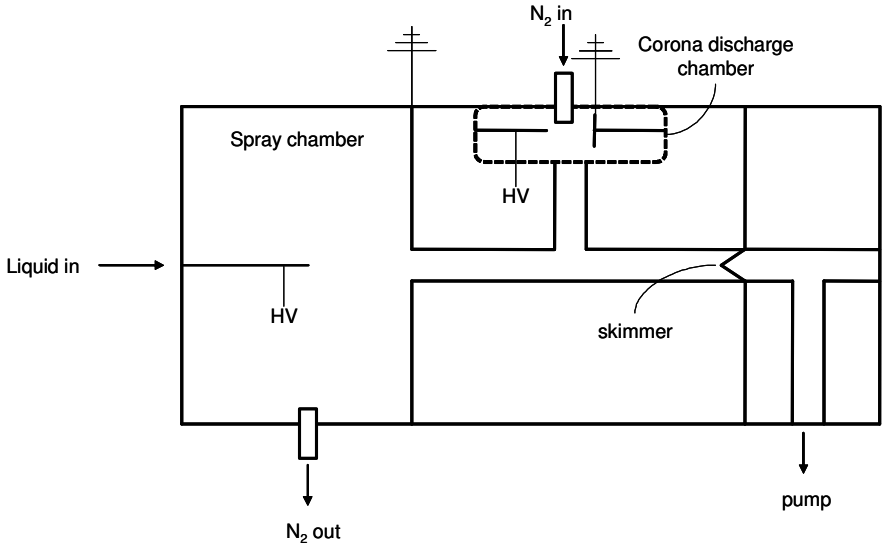

Figure 29: Schematic of entire electrospray apparatus developed for ESI of metal nanoparticles.

The apparatus is divided into three chambers; the spray chamber which is maintained at atmospheric pressure, the middle chamber which allows the aerosol to interact with the neutralizing gas, and the final chamber is at reduced pressure in order to interface with the matrix isolation apparatus.

The sample solution is introduced to the spray chamber through the electrospray capillary which is held at a high potential. This causes a charge separation in the solution, which forms a Taylor cone at the tip of the capillary. The jet which results from the Taylor cone is aimed through the counter electrode, which is grounded.

A counter propagating bath gas is fed into the system through the corona discharge chamber which allows for it to be charged to neutralize the sample spray. If the bath gas is not charged, i.e., if the corona discharge isn't produced, then electromagnetic 'lenses' could be used to further aid in the direction of the charged particles and ions. The particles pass through the bath gas which promotes evaporation of the remaining solvent before the sample reaches the final chamber.

The final chamber introduces the pressure differential to prepare the sample for introduction into the matrix isolation chamber. The spray passes through a sample cone to aid in the reduction of the pressure before it reaches the final chamber. A rotary pump is attached to this section to reduce the pressure further, before the remaining sample passes through a skimmer cone and flows into the matrix isolation apparatus.

2.2.1 Corona Discharge

The first attempt at achieving a corona discharge resulted in electronic discharge occurring from the base of the needle to the casing. The experimental setup consists of a Faraday cage surrounding a needle and plate held approximately two millimetres apart. This distance was chosen to make sure that the grounded plate was closer to the needle tip than the Faraday cage, which was roughly 5 mm away from the needle. The bath gas chosen was nitrogen gas as it was readily available and inexpensive. The gas was introduced at a high flow rate past the discharge chamber. Before the potential that was sufficient to ionize the gas, discharging occurred from the

pin to the grounded casing. The necessity to insulate the pin from its casing was determined, which was a difficult prospect due to the small space between them.

The first method attempted was to use electrical tape as an insulator, but due to the depth the pin was recessed into the casing, it wasn't possible to insulate to the base, therefore the system was still shorting. It was clear that a rigid insulator which could be pushed into the space was what was necessary. It was discovered that a small length of Nalgene tubing worked for this purpose and successfully filled the gap and prevented to shorting problem.

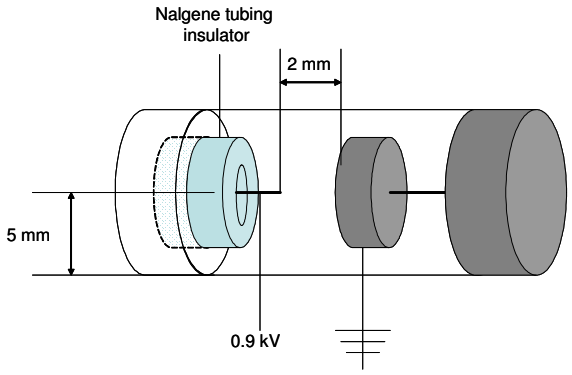

Figure 30: Graphical representation of corona discharge chamber of ESI apparatus.

The experiment was performed again, with all the conditions being kept the same with the addition of the tubing insulator. The potential applied to the pin was gradually increased until, at 900 V and with a high gas flow, a corona discharge was visible. It was determined that once formed, it was possible to drastically reduce the flow of gas without compromising the corona.

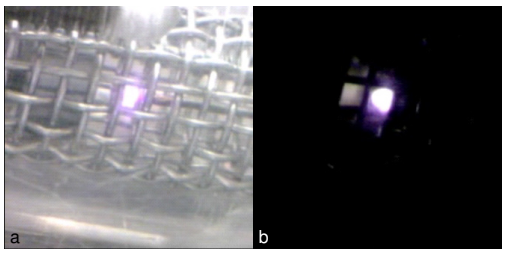

Figure 31: Photographs taken of N_2 corona discharge with a) room lights on and b) all lights off to improve appearance of corona.

2.2.2 Taylor Cone formation

The next component which was tested was the actual electrospray chamber. It was tested with both solvent test solutions as well as nanoparticle solutions.

The first solution used for testing was a 0.5 mM sodium citrate solution in 50:50 methanol: water mixture. Initial testing involved the test solution being in an open beaker with a length of PEEK tubing leading from it to the capillary. Within the ESI chamber the end of the capillary was kept approximately 10mm from the grounded counter electrode plate. There was no counter propagating gas in the chamber; it was simply left open to the atmosphere. When the potential was gradually increased on the capillary there was no sign of any change in the system, it was determined that due to both vessels being kept at atmospheric pressure, there was no force on the solution driving it into the capillary. The initial solution to this was to momentarily apply vacuum to the chamber, just until a droplet of solution is seen at the capillary tip. The pump was then shut off and removed from the chamber, leaving the capillary full of solution. The vacuum could not be left on as once the potential increased sufficiently, electrical discharge between the capillary and the grounded counter electrode occurred.

With a length of tubing measuring 18 inches, a stable Taylor cone could be achieved using these conditions. As the applied potential on the capillary was increased to approximately 3.5 kV, a Taylor cone-like shape could be seen, and as the potential was reduced, this shape prevailed as low as 2.2 kV. This method, while successful, released too much solution after the initial vacuum was applied. To circumvent this problem, the tubing was lengthened to 5 feet in order to slow the initial onslaught of solution. This however had no significant effect on the Taylor cone formation or the electrical potential requirements.

In order to solve the flow rate problem, while also giving more control, a syringe pump was employed. A stable cone was achieved using the citrate solution, with a flow rate of 10

μL/min. The counter electrode was set at -0.2 kV which allowed for a lower potential to be applied to the capillary, only 2.3 kV.

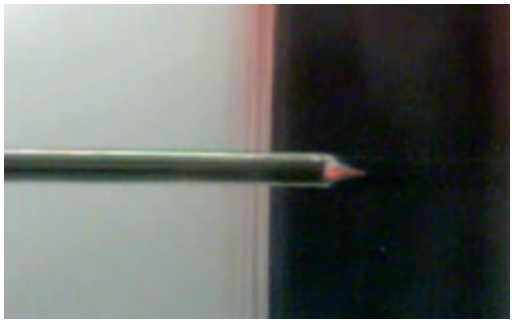

Figure 32: Picture taken of successful Taylor Cone formation using 0.5 mM sodium citrate in 50:50 (v/v) MeOH: H_2O.

2.2.3 In-situ testing

For testing of the entire system, it was decided that a residual gas analyzer (RGA) would be used to determine if any of the sprayed solution were to have made it through. It was quickly determined, however, that the vacuum achieved by attaching a rough pump to the final section of the system yielded insufficient vacuum for the safe running of the RGA. A second pump was attached to the electrospray chamber and a pressure of 30 mtorr was attained. When it was attempted to spray under these conditions it was quickly determined that a Taylor cone cannot form unless the electrospray chamber is at atmospheric pressure. This was possible to achieve with vacuum if the pressure from the N_2 from the corona discharge section were at a high enough flow, without exposing the system to actual atmosphere. As the final setup was to involve using matrix isolation and FTIR spectroscopy, it was determined that the increase in pressure would not be harmful to the system and, if the excess gas was nitrogen, it would not risk the introduction of water.

Before it was possible to couple the electrospray apparatus with the matrix isolation FTIR system, there were many problems with the IR system which needed to be resolved. Some of the

problems included: pressure problems with the helium compressor needed to cool the salt window, vacuum leaks within the FTIR apparatus as well as problems with some of the gauges. The time required to solve these problems was determined to be longer than it was prudent to wait due to the time constrictions of the degree, therefore alternative methods were looked at for this project.

References for Chapter 2

1. Lenggoro IW, Lee HM, Okuyama K. Nanoparticle assembly on patterned "plus. J Colloid Interface Sci 2006 NOV 1;303(1):124-30.

2. Schulz F, Franzka S, Schmid G. Nanostructured surfaces by deposition of metal nanoparticles by means of spray techniques. Advanced Functional Materials 2002 AUG;12(8):532-6.

3. Rauschenbach S, Stadler FL, Lunedei E, Malinowski N, Koltsov S, Costantini G, Kern K. Electrospray ion beam deposition of clusters and biomolecules. Small 2006 April 2006;2(4):540-7.

4. Richardson MJ. Direct observation of polymer molecules. Nature 1963 April 20, 1963;198:252-3.

5. Fenn JB. Electrospray ionization mass spectrometry: How it all began. J Biomol Tech 2002;13(3):101-18.

6. Dole M, Mack LL, Hines RL. Molecular beams of macroions. J Chem Phys 1968 Sept 1 1968;49(5):2240-9.

7. Signorell R, Kunzmann MK, Suhm MA. FTIR investigation of non-volatile molecular nanoparticles. Chemical Physics Letters 2000 October 13, 2000;329(1-2):52-60.

Chapter 3

Sol-Gel Encapsulation

Sol-gel encapsulation was chosen as the next method for nanoparticle isolation due to its similarities to matrix isolation. A gel can behave as a matrix, in that it allows gases to penetrate the gel and access the species, in this case metal nanoparticles, which are trapped inside. The gel would allow the small molecules to interact with the nanoparticles, while preventing the nanoparticles from agglomerating. The gels are optically transparent which would allow spectroscopic analysis, thus it wouldn't be necessary to rethink all the aspects of the project.

3.1 Literature Review

Sol-gel materials have been used extensively in the field of optical devices, not because they offer new optical properties, but because they can be used to make existing materials in a different way.[1] Sol-gel materials are most commonly used in two ways, either as a thin film coating, or as a bulk material. Thin films are used extensively on their own for various optical coatings, ranging from filters and antiglare coatings to the production of mirrors through the use of many layers. The sol-gel process gives developers a high degree of control over the thickness of the coatings as well as its composition. More often in recent applications, the gels are used more as a rigid host for the encapsulation of other, optically active, species.

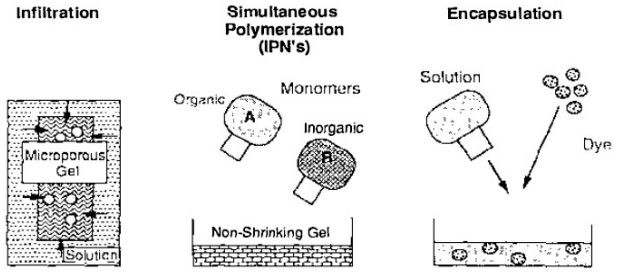

Figure 33: Diagram of sol-gel materials as rigid hosts, with method for the introduction of chromaphores.[1]

When used in this way, the important property of the sol-gel is that it is optically transparent. In this way, the sol-gel is used as a matrix which controls the size and homogeneity of the contained species. In the case of spectroscopy, silica gel is optically transparent to about 250 nm, which makes it an ideal candidate for these types of applications.

Sol-gel encapsulation is a relatively new concept, having only received focus in the last decade. Prior to this, the most common methods of trapping species of interest was through adsorption onto a surface, or through covalently bonding them to one.[2] Having the molecule of interest adsorbed onto a support had the advantage of being an easy and versatile process, but leaching into the surrounding was highly probable which reduced the lifetime of the sample, and contamination of the surroundings. Covalent bonding solved the problem of leaching, as it formed a permanent bond between the surface and the sample, but restricted the geometry of the molecule. In the case of biomolecules and enzymes, this would often reduce their activity. Sol-gel encapsulation solved these problems by trapping the molecule within the pores of the rigid gel thus greatly reducing the likelihood of leaching while still giving them the steric freedom for rearrangement. It is also an easy process with mild reaction conditions which aid in the preserving of less stable molecules. Many molecules of interest are synthesized in the solution phase and are not stable when removed. The sol-gel process allows for their inclusion in the solid during the gelation phase so that the sample never needs to be removed from solution. The

porosity of the gel allows access to the molecule of interest for sensing and reaction purposes. Depending on the gel process used, the rigid host may continue to shrink over time, due to condensation. If medium to large molecules are infiltrating the gel, this could reduce their ability to access the trapped molecules, but for small molecules the pores remain large enough for this purpose.

Metal nanoparticles are often encapsulated in this way. Most commonly, the metal salt is introduced to the sol and then reduced once the gel has solidified. One example of this is the work done by M. Zayat, where Ag NPs were produced in situ in a borosilicate glass by the sol-gel method.[3] A silver chloride solution (AgCl) was present during the formation of the sol-gel, so that once solidified, Ag^+ ions occupied the pores of the gel. The solid was then exposed to sunlight, which caused a darkening of the films due to silver reduction. Another reduction method used was by heating the gel to 600 °C which caused the gel to adopt the pale yellow colour typically associated with quantum dots and small nanoparticles.

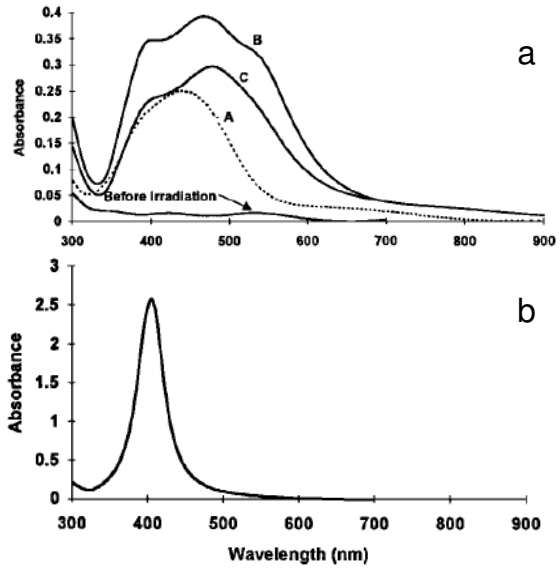

Figure 34: SPR spectra of silver particles encapsulated in sol-gel a) various amounts of AgCl in sol-gel before and after irradiation with sunlight. b) AgCl after gel was heated to 600 °C.[3]

Selvan et al. used a slightly different method where TMOS was added to a gold chloride hydrosol.[4] Ammonia was added after about an hour of TMOS addition and the resulting gel contained Au NPs as confirmed using SPR.

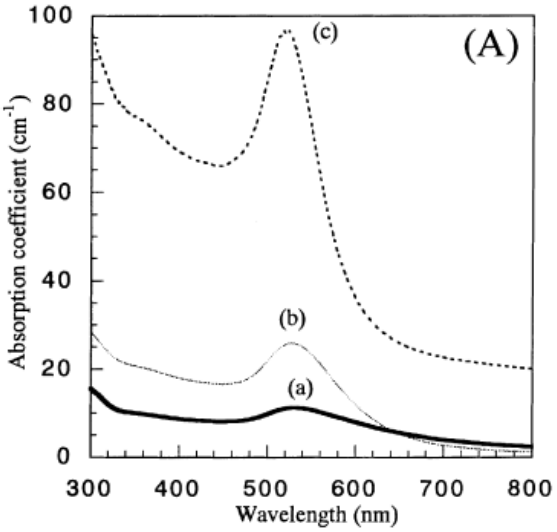

Figure 35: SPR spectrum of Au containing gels produced by Selvan et al, each spectrum consists of increasing amounts of Au.[4]

This method had both the gelation and the reduction of the metal occurring simultaneously. There was no sign of agglomeration in the particles which indicate successful encapsulation. The problem that can arise using this method is that, in the case of organic gels, the functionality of the gel itself can be compromised or even destroyed.[5] This leads to the most recent method used, which is to incorporate already formed nanoparticles into the gel. Vreugdenhil et al. successfully encapsulated laser ablated Au NPs into organic gels, with only slight agglomeration.[5] This method allowed for the gel to maintain all its functionality as the only change to the synthesis was that there was extra water present due to the addition of the nanoparticle solution.

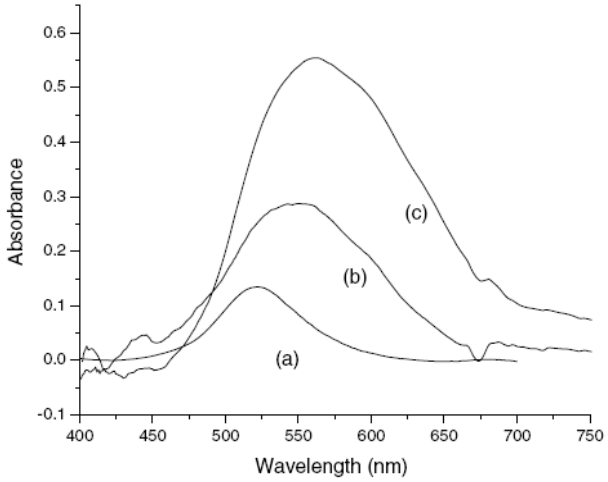

Figure 36: SPR of Au NPs in a) solution b) low concentration in gel c) high concentration in gel.[5]

It is believed that arrested agglomeration is the cause for red shift of the surface plasmon, wherein the nanoparticles and methanol are excluded during the gelation process and are thus forced closely together in the voids of the gel. At low concentrations, the degree of agglomeration is greatly reduced, which supports this postulate.

3.1.1 Metal Nanoparticle interactions with CO

Carbon monoxide is one of the simplest IR active molecules. It is often chosen as the sample molecule used as a surface probe for metal surfaces as it will bind with the metal in various orientations and is a good model for more complicated surface reactions.[6] In 1954, R. P. Eischens was able to observe the CO-M interaction for various metals.[7] It wasn't until several years later that he realized the 'metal slurry' that he had made was in fact metal nanoparticles.

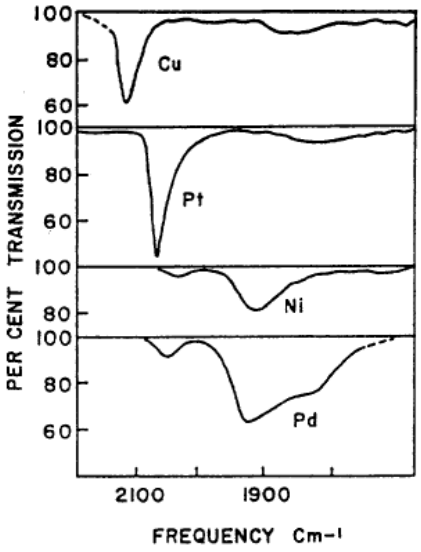

Figure 37: IR spectra of chemisorbed CO on metal nanoparticles.[7]

M. Mucalo added to this library of metals by investigating the FTIR spectrum of CO adsorbed onto Au NPs.[8] Where salt reduced gold nanoparticles were exposed to both ^{12}CO and ^{13}CO to determine the features associated with surface interactions.

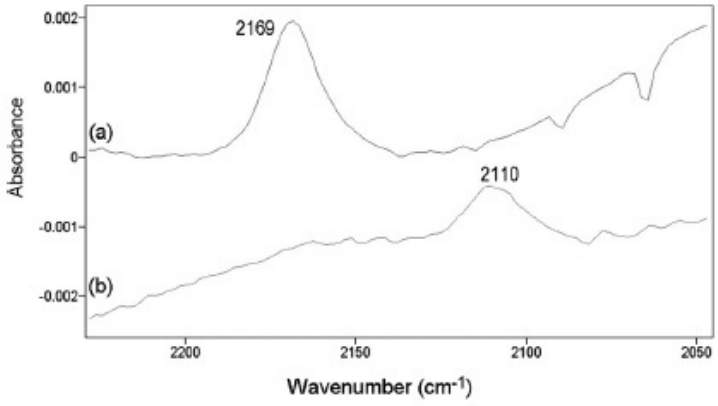

Figure 38: FTIR spectrum of CO-Au interactions of surface adsorbed CO. a) sample containing ^{12}CO, b) sample containing ^{13}CO.[8]

3.2 Experimental

3.2.1 Nanoparticle Synthesis

The most common method for the production of gold nanoparticles (Au NPs) uses sodium citrate as both the stabilizing agent as well as the reducing agent. The process followed is the same found in the article written by McFarland et al.[9] A 0.1mM gold salt solution was produced through dissolving 0.0163 g gold chloride ($AuCl_3$, Sigma-Aldrich, ACS reagent) in 41mL distilled water; water which was used for all nanoparticle synthesis. The resulting yellow solution was heated to a vigorous boil with stirring. A second solution, 38.8 mM sodium citrate achieved through dissolving 0.0673 g sodium citrate (Sigma, ACS reagent $\geq$ 99% purity) in 4.1 mL water, was added at once to the gold solution. It was left on the heat for an additional 10min, in which the solution went through a colour change from yellow through blue before turning a deep burgundy colour which remained. The solution was then removed from heat and allowed to cool. In the case where the solution was to be made more concentrated, the solution was allowed to boil until the desired volume was achieved. It was determined that the Au NPs could be concentrated by three times and retain their stability. The success of the synthesis was determined through the SPR peak, which was seen at a wavelength of 520 nm.[9]

Another method for producing Au NPs adopted from Nutt, using tannic acid along with sodium citrate was also used.[10] This process has the distinction of supposedly making smaller diameter nanoparticles, which according to the authors would be on a size scale of approximately 6nm. This process used a 0.36 mM gold solution prepared by dissolving 0.0144 g $AuCl_3$ in 80 mL water. The reducing agent was composed of 0.004 g sodium citrate, 0.005 g tannic acid (Sigma Aldrich, ACS reagent) and 0.0018 g potassium carbonate (Aldrich, 99.995%) dissolved in 20 mL water. Both solutions were heated simultaneous to 60 °C, with stirring, before the brown

tannic acid solution was added to the pale yellow gold solution. The final solution was allowed to boil for two minutes before being removed off the heat. The SPR peak of the final solution appeared at 525 nm, indicative of the successful synthesis of Au NPs.[10]

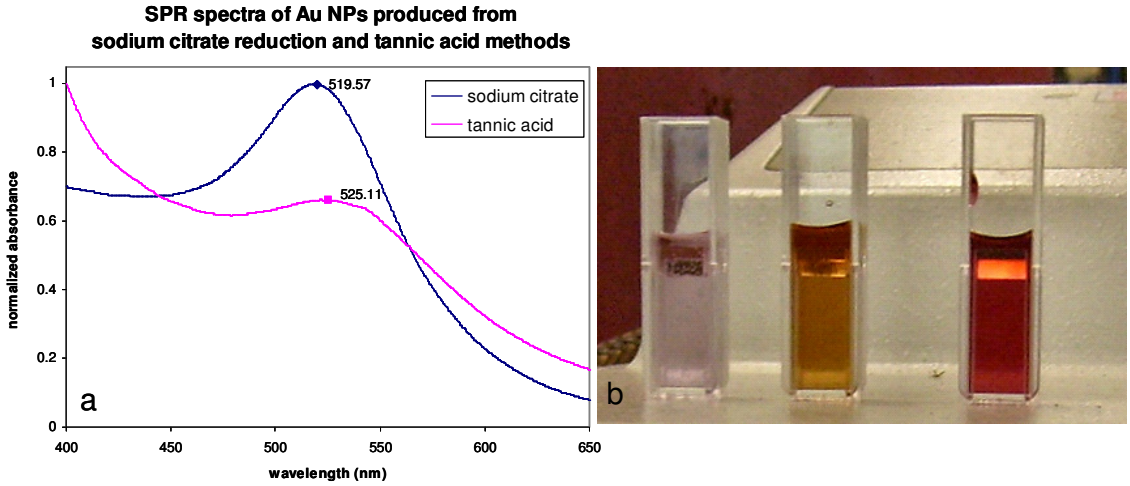

Figure 39: a) SPR spectra of Au NPs synthesized using sodium citrate and tannic acid methods. b) Photo taken of all three Au NPs solutions used; glucose, tannic acid and sodium citrate, in order.

This same method can also be used for the production of palladium nanoparticles (Pd NPs) with only minor modifications. While the reducing agent, the tannic acid solution, is identical in both syntheses the metal salt solution differs in both content and concentration. A 0.525 mM palladium salt solution is produced by dissolving 12 mL palladium chloride ($PdCl_2$, Sigma-Aldrich, 5% wt in 10% wt HCl). Once again, both solutions were heated to 60 °C before the tannic acid solution was added to the palladium solution. The solution was allowed to boil for 25 min before being removed from the heat and allowed to cool. The brown Pd solution was then allowed to sit overnight before being used, during which the solution turned a deep coffee brown/black colour. The SPR of Pd NPs of this size, approximately 4nm according to Nutt, is difficult to say for certain but has been reported in the range of 267 – 281 nm.[11] When taking the

SPR of Pd NPs, there is absorbance due to the tannic acid in the same region, but a peak at 271 nm can be seen.

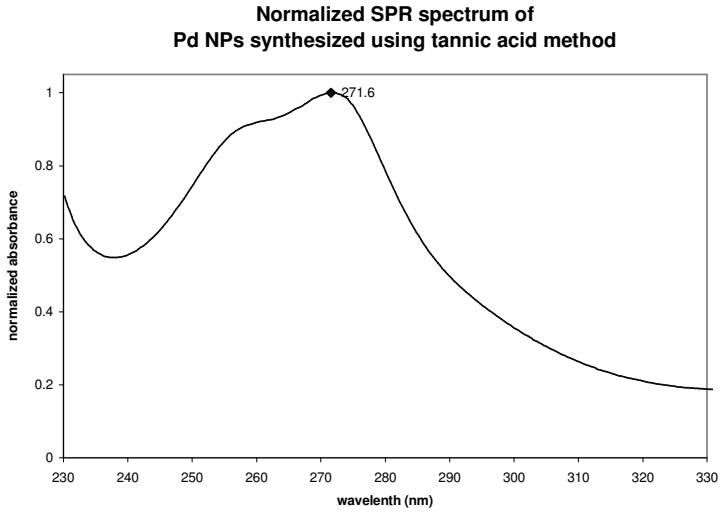

Figure 40: SPR spectrum of Pd NPs synthesized using tannic acid method.

The final method used for the synthesis of Au NPs was classified as a 'green' technique, as the reducing agent used was glucose.[12] A 27.7 mM sugar solution was made by dissolving 0.2000 g of glucose (d+ glucose, Sigma, ≥ 99.5%), or for smaller particles fructose (d fructose, Aldrich, 99+%), in 4 mL water. A volume of 100 μL of 10^{-2} M gold salt solution was added directly to it. It was then heated to 70 °C in a hot water bath and remained for approximately five minutes, until a notable colour change occurred. The SPR was again observed at 520 nm in the case of glucose, and 515 nm when fructose was used. It was determined that if there were any residue on the glassware, the particles would not remain suspended due to the weak protection yielded by the sugar molecules.

This process could also be used for the synthesis of silver nanoparticles (Ag NPs) by simply substituting 100 μL of 10^{-2} M silver nitrate ($AgNO_3$, Sigma-Aldrich, 99.9999%) and leaving all other conditions the same. The resulting SPR was seen as a weak feature at 400 nm.[13]

A more recognized method for the synthesis of Ag NPs would be that of the sodium borohydride method.[13] A 1.0 mM silver salt solution was made by dissolving 0.0066 g $AgNO_3$ in 39 mL of water. The reducing solution was produced by dissolving 0.0065 g of sodium borohydride (Sigma Aldrich, Reagent Plus) in 86mL of water. The reducing solution was chilled in an ice bath for 20 min with stirring. The silver solution (5.7 mL) was added drop wise, to the reducing solution; the stirring was stopped immediately once all the silver solution was added. The resulting solution turned a bright shade of yellow, which darkened over time. The existence of Ag NPs was confirmed through the observation of the SPR peak at 397 nm.

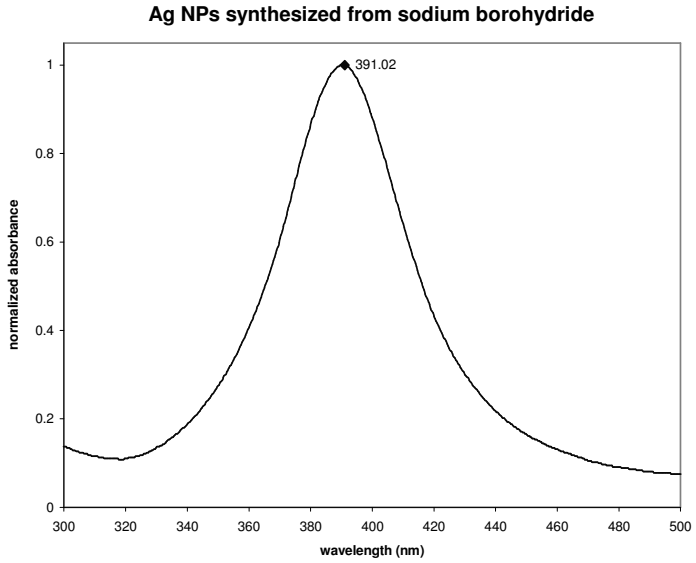

Figure 41: SPR spectrum of Ag NPs synthesized using sodium borohydride reducing agent.

The final method used was for the synthesis of platinum nanoparticles (Pt NPs) and used a combination of sodium borohydride and sodium citrate reducing agents.[14] A 2.5 mM platinum salt solution was made in advance by dissolving 0.0218 g of chloroplatinic acid (H_2PtCl_6, Aldrich, ≥99.9%) in water. The solution was allowed to age, with stirring, for 29 hr. Once aged, 0.0036g of sodium citrate was added and stirred for 5min, followed by an addition of 0.0056 g of sodium borohydride; the solution immediately turned a dark brown but was left to stir for 20 min

longer. An SPR feature was seen at 217 nm, which was near the edge of the spectrometers detection limit.[15]

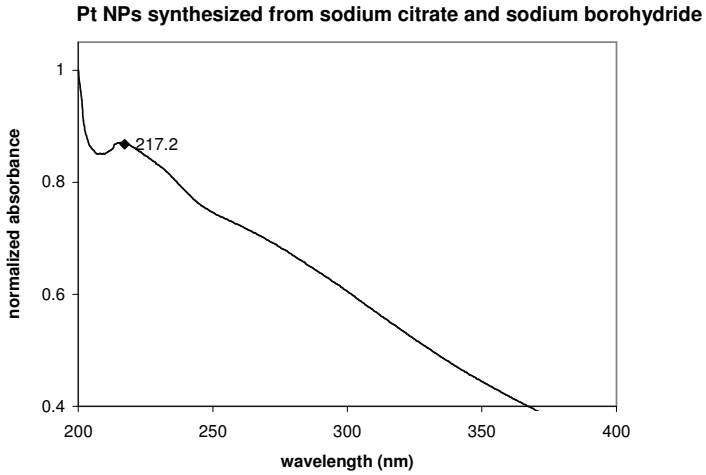

Figure 42: SPR spectrum of Pt NPs synthesized using sodium citrate and sodium borohydride.

3.2.2 Sol-gel synthesis

The method used for organic sol-gel synthesis was a 3:1 GT gel as established by A Vreugdenhil.[16] A solution composed of 14.20 mL of 3-glycidoxypropyltrimethoxysilane (GPTMS, Aldrich 98%) and 2.96 mL trimethoxysilane (TMOS, Aldrich 98%) was added drop wise to 21.60 mL of 0.05 M acetic acid solution. This process took on average two hours. Once all the sol had been added to the acidified water, the solution was allowed to age with stirring for three days. At this point, 19.38 mL of Fluorad surfactant was added along with, in the case of a nanoparticle containing gel, 15 mL of nanoparticle solution. Meanwhile, in a separate container, 1.38 mL of both diethyltriamine (DETA, Aldrich 99%) and water were mixed before being added quickly to the sol. In making monoliths, at this point the sol would be poured into Petrie dishes and allowed to solidify. While drying, the solid monolith would shrink in size as the solvent

evaporated, this would be promoted until the monolith would be of an appropriate size to fit into the gas cell used for the FTIR experiments.

If the gel were to be used for coatings, a silicon wafer which was previously prepared would be mounted in an automatic dip-coater which would lower and raise the slide into the sol-gel solution in a steady, controlled manner. The slide would be dipped three times before being removed from the system and hung on a line to dry.

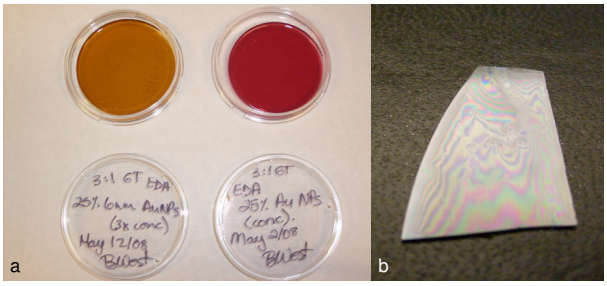

Figure 43: Organic sol-gels containing gold nanoparticles a) monoliths containing two different sizes of Au nanoparticles and b) silicon wafer dip-coated with a thin film of sol-gel containing gold nanoparticles.

The silicon wafers were cleaned in three steps, following the RCA cleaning protocol. This method involves two different chemical baths to remove organic and metallic contaminants from the silicon surface. The first bath, geared towards the removal of organic residue, consists of ammonium hydroxide (Caledon 28.0-30.0%), hydrogen peroxide (Fisher 30% certified ACS) and water in a ratio of 1:1:5. The solution is heated to 70 °C and the slides are allowed to soak for at least 15 min. The slides are removed from the bath and are rinsed with deionized water. The next bath is very similar to the first, except hydrochloric acid (Caledon 36.5-38%) is used instead of ammonium hydroxide, and the ratio is 1:1:6 (HCl: H_2O_2: H_2O). All other conditions are the same as the previous step for this treatment to remove dissolved metals. Once the slides were rinsed, they were allowed to air dry and used for dip coating shortly there after.

In comparison to organic gels, the inorganic variety is much simpler from a chemical standpoint.[17] A volume of 5 mL of triethoxysilane (TEOS, Aldrich reagent grade 98%) was mixed with 5.1 mL of ethanol and this solution was then heated to 70 °C with stirring. Once heated, 4.1 mL of 0.165 M hydrochloric acid was added, and the solution continued to stir for an additional 30 min. The gel eventually solidified through evaporation after 3 days. Inorganic gels can also be base catalyzed, using sodium hydroxide (Caledon, 28.0-30.0%) instead of hydrochloric acid and keeping all concentrations and amounts the same. Sodium hydroxide was chosen instead of ammonium hydroxide, which was used by the authors, to prevent any interaction with the metal nanoparticles once they were introduced.

3.2.3 Gas Handling System

For the introduction of gas samples, an all metal gas handling system was employed. Once the system was sealed, a rotary pump was used for the initial pumping stage which reduced the pressure of the line down to 5.0×10^{-2} torr, which was measured using a Pirani gauge. When this pressure was achieved a diffusion pump would be used to further reduce the pressure of the system to 10^{-7}torr which was monitored using a cold-cathode sensor.

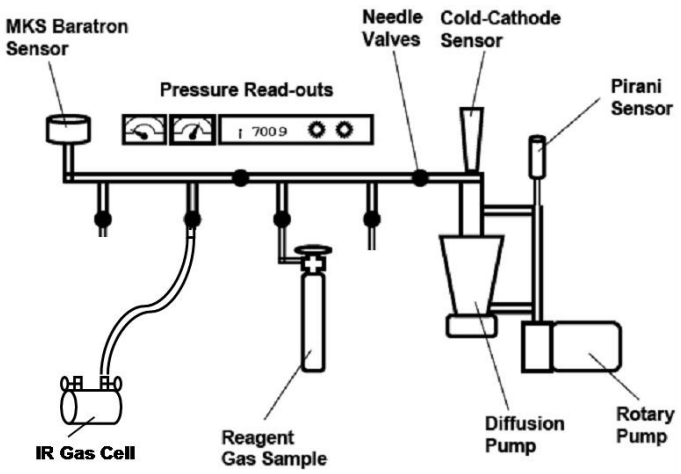

Figure 44: Schematic of gas handling system.

A MKS Baratron sensor was also present to facilitate the addition of samples as it would measure pressures of 10^{-1} – 10^{2} torr. The flow of the samples was controlled by needle valves present at every junction in the line; they were used for both the direction of the flow as well as the rate.

3.2.4 Experimental Procedure

A glass IR gas cell was used for all the sol-gel experiments. Two Teflon rings were machined to hold the monolith, or Si slide, upright in the path of the IR beam; channels were carved in the rings to allow the gas to fill the entire cell, and to prevent a difference of pressure on either side of the sample.

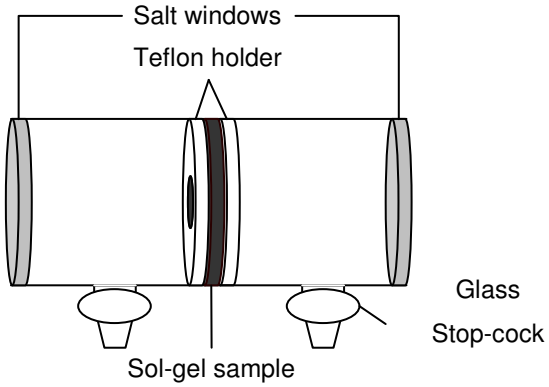

Figure 45: Graphical representation of gas cell used for sol-gel experiments.

The gas cell could be attached to the gas handling system in order to be purged and filled with the gas sample. For samples containing a dip-coated slide, the gas cell would be open to the line to be purged simultaneously. Once the pressure of the entire system reached 10^{-7} torr it was considered purged, there was no additional wait time. In the case of a sol-gel monolith, for UV/vis experiments, the cell would not be exposed to vacuum, instead it would be purged with nitrogen gas (N_2, Praxair) at a moderate flow rate. This method was chosen due to fact that the monolith fractured extensively when exposed to vacuum; it was no longer optically transparent. The gas is allowed to flow for at least 20 min before it's considered 'clean'; a reference spectrum

would then be taken. Once the reference spectrum has been collected, the gas cell was reattached to the gas line for the introduction of the gas sample. Carbon monoxide (CO, Matheson, 99.998%) was attached to the line, and its connection as well as the gas cell connection was purged. The needle valve above the CO lecture bottle was sealed after purging; the gas tank was opened briefly to pressurize this small section of pipe, then immediately closed again to prevent waste. The needle valve would then be opened gradually and the line would be pressurized to 760 torr. The gas cell would be sealed and removed from the line; it would then be left for 30min before the gas would be removed. The cell would be purged with N_2 gas, to prevent the removal of weakly adsorbed molecules. The N_2 gas would be allowed to flow through the cell for approximately five minutes, before the cell was again sealed and the sample spectrum would be taken.

3.3 Results

3.3.1 Sol-gel encapsulation

When attempting to encapsulate the metal nanoparticles in the GT gels, it was first attempted without any additional modifications to the gel process. The nanoparticles were introduced to the sol just before the cross linker was added. SPR spectroscopy was used to determine the stability of the nanoparticles after the gelation process had finished.

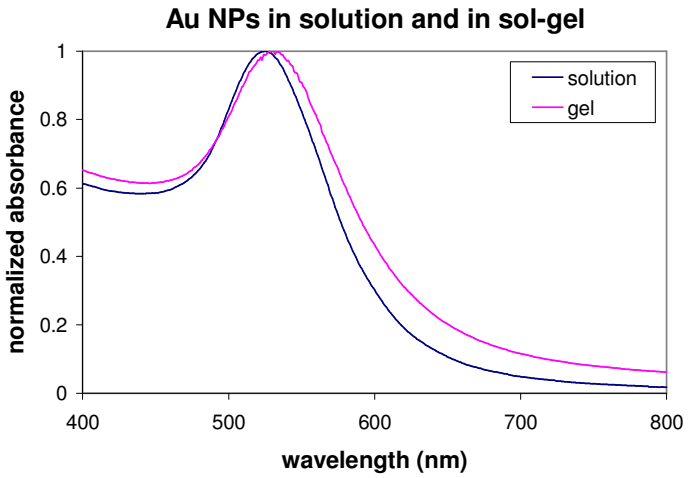

Figure 46: SPR spectra of Au NPs before and after sol-gel encapsulation.

It can be seen that the SPR peak was red shifted only very slightly, which indicates that the particles themselves did not suffer any great degree of agglomeration or destabilization. All four metals tested; Au, Ag, Pd and Pt, were successfully encapsulated without modifying the sol-gel process.

Inorganic gels were also produced, with less promising results. First, the acid catalyzed gels were synthesized. The gelation process was predominantly due to evaporation, due to the lack of cross linker. The resulting gel was very brittle and would crack during the drying process which reduced its optical clarity. Various attempts were made to improve the durability of the gel; most notable was the addition of stainless steel mesh to the gel. It was thought that the mesh would act as reinforcement for the gel, thus preventing the fractures. What happened, however, was that the gel pulled away from the mesh while drying, due to the natural shrinkage of the gel. Base catalyzed gels did not suffer the same problem of rapid shrinkage and solidified much faster. The primary problem with the base gels was the loss of optical clarity due to cloudiness. The gel became flaky in consistency and was no longer transparent. Dip coating silicon slides with the

inorganic gel was also not possible due to the slow drying time; all the gel would drip off the slides before the gelation was complete.

3.3.2 CO exposure with sol-gel encapsulated nanoparticles

Organic sol-gel monoliths each containing a different metal nanoparticle, either by metal (Au, Ag, Pd, Pt) or by method (citrate, tannic acid etc.) were exposed to CO gas for 1hr before being purged with nitrogen. When the FTIR spectrum was obtained, it was determined that the monoliths were too thick, as all the radiation was absorbed. Thin films on Si wafers were subsequently used, with all other conditions remaining the same. There was a high degree of periodic interference in the spectra which made making any definitive conclusions difficult. When looking at the spectra produced by the various samples containing Au NPs an anomaly in the noise was seen at 2169 cm^{-1}.

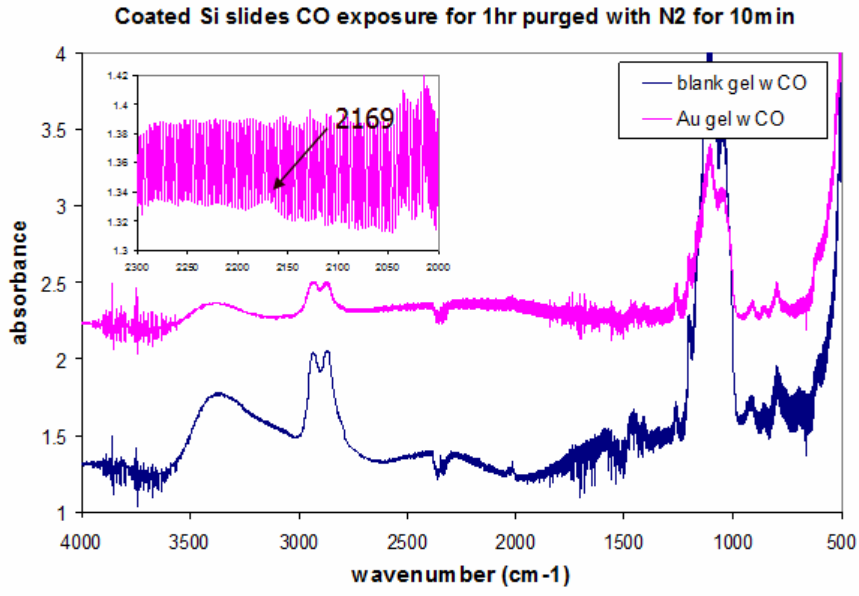

Figure 47: Spectra of Sol-gel slides containing Au NPs and no particles after exposure to CO. Insert is a magnification of 2000-2300 cm^{-1} region of Au NPs sample indicating the anomaly at 2169 cm^{-1}.

This anomaly was absent in all other samples both without particles and with the other metals. When the concentration of the particles was increased threefold in the gel, the anomaly also increased; the noise was still too large to make any further determinations. Any attempt to mathematically improve the signal, by creating a filter for the periodic interference, was unsuccessful as well.

The monoliths were also used for UV/vis experiments. As the gels are optically transparent up to 250 nm, only gold and silver nanoparticles were used as the surface plasmon absorption of platinum and palladium are too low wavelength to be seen. For both metals and for various concentrations there was no change in the SPR peak before and after the exposure to CO. The exposure time was extended from 1hr to approximately 24 hrs with no change.

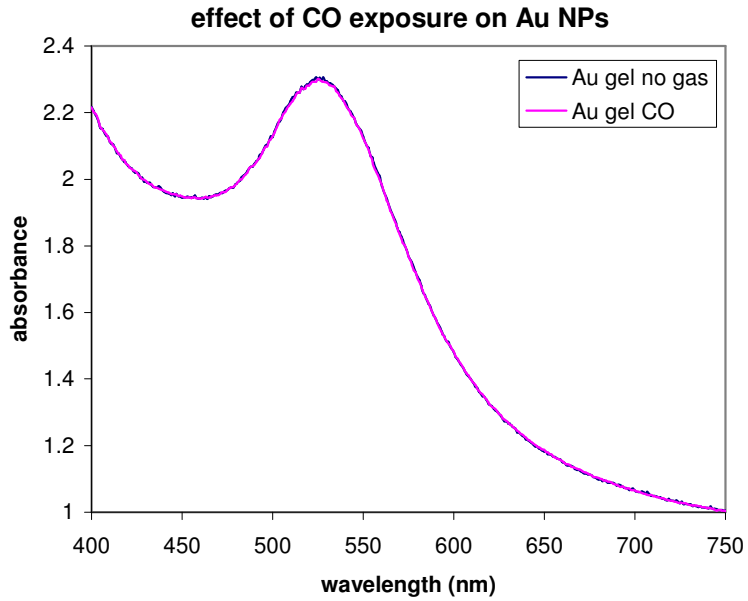

Figure 48: SPR spectra of Au NPs before and after 1hr exposure to 1atm CO.

3.4 Discussion of Results

Metal nanoparticles were successfully synthesized from various methods and with various metal contents. They were successfully characterized through the confirmation of their

SPR peaks. Once synthesized, it was possible to suspend the particles in an organic gel with only minute changes to the surface plasmon, which indicates a minor degree of agglomeration. When attempting to make inorganic sol-gels, believed to improve the FTIR experiments by reducing the amount of IR active species, there were many problems which arose. The acid catalyzed gels were very brittle and shattered while drying due to the fragility and the rate of shrinkage. Any attempt made to reinforce the gel proved fruitless. When a base catalyzed gel was attempted, the result was a more porous gel which didn't shrink nearly as much. The problem with this gel was that its final appearance was opaque and had a flakey quality. As it was no longer optically transparent, it was not useful for the application.

Even though no definitive results can be made based of the FTIR results, due to the high degree of noise, the anomaly present in the Au NPs samples could be of interest. It is known that Au-CO interactions do have a vibrational feature present at 2169 cm^{-1} but with the amount of noise it is impossible to say if this peak is the cause of the abnormality.[8] The lack of change in the UV/vis experiments indicates that any interaction between the particle and CO, it has no significant effect on the electronic structure of the nanoparticle itself.

References for Chapter 3

1. Klein LC. Sol-gel optical materials. Ann Rev Mater Sci 1993;23:437-52.

2. Lin J, Brown CW. Sol-gel glass as a matrix for chemical and biochemical sensing. Trac-Trends in Analytical Chemistry 1997 APR;16(4):200-11.

3. Zayat M, Einot D, Reisfeld R. In-situ formation of AgCl nanocrystallites in films prepared by the sol-gel and silver nanoparticles in silica glass films. J Sol Gel Sci Technol 1997 June 1997;10(1):67-74.

4. Selvan ST, Nogami M, Nakamura A, Hamanaka Y. A facile sol-gel method for the encapsulation of gold nanoclusters in silica gels and their optical properties. J Non Cryst Solids 1999 OCT;255(2-3):254-8.

5. Vreugdenhil AJ, Pilatzke KK, Parnis JM. Characterization of laser ablated gold nanoparticles encapsulated in epoxy amine crosslinked sol-gel materials. J Non Cryst Solids 2006 OCT 1;352(36-37):3879-86.

6. Poon HC, Saldin DK. A molecular representation of the potential of carbon monoxide adsorbed on a nickel surface. J Phys : Condens Matter 1989;1:1551-9.

7. Eischens RP. Early days in the infrared study of adsorbed molecules. Colloids and Surfaces A-Physicochemical and Engineering Aspects 1995 DEC 1;105(1):87-93.

8. Mucalo MR, Babu KM, Wu KSW. In situ characterisation of the aqueous gold colloid interface using CO as a surface probe: IR spectroscopic studies. J Colloid Interface Sci 2007 JUN 1;310(1):184-9.

9. McFarland AD, Haynes CL, Mirkin CA, Van Duyne RP, Godwin HA. Color my nanoworld. J Chem Educ 2004 April 2004;81:544A.

10. Nutt MO, Heck KN, Alvarez P, Wong MS. Improved pd-on-au bimetallic nanoparticle catalysts for aqueous-phase trichloroethene hydrodechlorination. Applied Catalysis B, Environmental 2006 December 1, 2006;69(1-2):115-25.

11. Wu Y, Zhang Y, Zhang L. Effects of finely dispersed metallic palladium on microstructure and properties of nanocomposites produced by sol-gel technique. China Particuology 2004 2;2(1):19-24.

12. Panigrahi S, Kundu S, Ghosh SK, Nath S, Pal T. General method of synthesis for metal nanoparticles. Journal of Nanoparticle Research 2004 AUG;6(4):411-4.

13. Solomon SD, Bahadory M, Jeyarajasingam AV, Rutkowsky SA, Boritz C, Mulfinger L. Synthesis and study of silver nanoparticles. J Chem Educ 2007 FEB;84(2):322-5.

14. Hussein AS, Murugaraj P, Rix C, Mainwaring D. Mechanism of formation and stabilization of platinum nanoparticles in aqueous solvents. Smart Materials II 2002 November 1, 2002;4934(1):70-7.

15. Gao Y, Zhang X, Li Y, Liu H, Wang Y, Chang Q, Jiao W, Song Y. Saturable absorption and reverse saturable absorption in platinum nanoparticles. Opt Commun 2005 7/15;251(4-6):429-33.

16. Vreugdenhil AJ, Woods ME. Triggered release of molecular additives from epoxy-amine sol–gel coatings. Progress in Organic Coatings 2005 6/1;53(2):119-25.

17. Nogami M, Moriya Y. Glass formation through hydrolysis of si(OC2H5)4 with NH4OH and HCl solution. Journal of Non-Crystalline Solids 1980 4;37(2):191-201.

Chapter 4
Other Methods

Based on the complications encountered with trying to promote the interaction of metal nanoparticles with gas phase small molecules, solution phase molecules were then studied. Two separate methods were attempted to this end; direct solution phase observation as well as glass surface support.

Direct solution phase observation was chosen for its ability to simplify the system. By allowing the nanoparticles to remain in solution, the need for stabilizers and support was removed. The latter were the main source of interference in the previous methods looked at in this project. It is also possible with the absence of a rigid matrix it would be possible to see more diverse interaction between the nanoparticles and the small molecules.

Glass surface support was chosen as the final method in the hope of increasing the concentration of the nanoparticles without the need for stabilizers, so that the number of interactions would increase and could possibly be observed spectroscopically. There would be no need for the solvent to be present during the spectroscopic analysis, which would reduce the amount of noise or interfering species and also aid in the observation of the interactions.

4.1 Literature Review

While there are several functional groups known to have high affinity with gold nanoparticles, two of these which are often studied are amines and thiols.[1] Due to their hydrophilic nature they are ideal for use in aqueous solutions and are often used to attach gold nanoparticles to rigid supports for various applications.[2]

The adsorption of ammonia on gold surfaces is of some interest with regard to the behaviour of clean gold surfaces compared to oxide coated ones. Lui et al. used computational

calculations to determine how ammonia interacts with these clean nanoparticles.[3] The authors calculated the binding energy associated with the adsorption of ammonia, both gas phase and aqueous, depending on the binding site on the particle. They were able to account for the hydrogen bonding of ammonia with water in aqueous systems and were able to determine the best binding sites to be those at surface defects on the particle, along ridges on the surface. They also demonstrated that the binding changes as the ammonia dissociates with a concomitant increase in the binding strength and a decrease in the N-Au bond length.

Thiols and sulfides are also often used for binding Au NPs. In 1983, R. Nuzzo and D. Allara investigated the binding of disulfides with gold nanoparticles. It was determined that the disulfides would bind to the particles through the cleavage of the S-S bond. This differs from other metals which will cleave the S-S bond or C-S bond, an effect which was attributed to the presence of oxides on the surface of the particles; gold nanoparticles do not oxidize under ambient conditions.

4.1.1 Surface Treatment

3-mercaptopropyltrimethoxysilane (MPTMS) is commonly used in conjunction with metal nanoparticles to create surface treatments for various applications. It is designed to adhere to glass or silicon surfaces through its silane functionality, while it can attach to metal nanoparticles with the sulphur atom. T. Bai and X. Cheng were able to use MPTMS to form a self assembled monolayer on a clean, polished silicon wafer.[4] It was determined that a perfect monolayer was obtained after a reaction time of 90 min. A similar process was used by Li et al. for the purpose of using MPTMS aerogels for Surface Enhanced Raman Spectroscopy (SERS) by having the silver nanoparticles adsorb onto the gel.[5] The success of the adsorption can be monitored by the disappearance of the S-H feature at a shift of 2577 cm^{-1} in the Raman spectrum of the MPTMS after exposure to the solution. These results were confirmed by Thompson et al.

who verified that MPTMS adsorbs onto Au and Ag metal surfaces through the S atom.[6] Its also stated that the MPTMS orients itself so that the sol-gel network is parallel to the metal surface, with the MTPMS back bone more or less perpendicular to both.

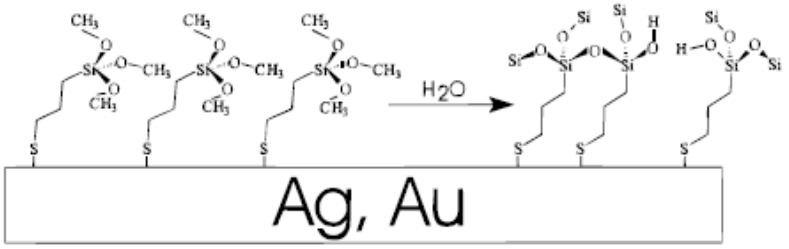

Figure 49: Schematic of MPTMS monolayer formation on metal support.[6]

4.2 Experimental

4.2.1 Au NPs experiments in solution

A 0.1 M solution of either ammonium sulphate (0.2013 g in 15.2 mL H_2O, Fisher, laboratory grade) or diethylamine (156 µL in 14.8 mL H_2O, Sigma-Aldrich, ≥99.5%) was made to be added to Au NPs solution. A range of concentrations of the solution (1% - 10% v/v) was added to 1 mL samples of Au NPs. The solutions were investigated using UV/vis spectroscopy and TEM and attempted with FTIR and Raman spectroscopy. For TEM samples, three drops of each solution to be tested were deposited one at a time on Formvar coated TEM grids (Soquelec, Cu 300 mesh) allowing each drop to dry in a desiccator for 15 min before the next drop was added.

4.2.2 Surface Treatment

A volume of 6.3 mL of 3-mercaptopropyltrimethoxysilane (MPTMS, Aldrich, 95%) was added dropwise to 120 mL water with stirring, and allowed to age for 30 min. The solution was then transferred to glass staining trays. Clean glass slides were added to the solution and allowed to soak for various lengths of time, ranging from 1 hr to 24 hr. Once removed, the slides were

hung to line dry overnight. The staining trays were then filled with Au NPs solution, either as made or in addition to either sodium dodecyl sulphate (SDS, Sigma-Aldrich, ≥99.0%) or sodium-1-decyl-sulfonate ($SC_{10}SO_3$, Sigma, approximately 98%) surfactant. The coated slides were then allowed to soak for 60 min before being removed and hung to dry, again, overnight. The coatings were confirmed by Raman spectroscopy after the MPTMS coating and the addition of Au NPs.

The protocol for cleaning the glass slides consisted of chemical baths and sonication. The glass slides were first sonicated in a methanol bath for approximately 5min, after which the slides were rinsed with Millipore water. The next step was to soak the slides in a glass cleaner (potassium hydroxide (KOH)/ethanol) bath for another 5min. After another rinse with water, the slides were sonicated in fresh Millipore water for 5-10 min before being hung to dry.

4.3 Results

4.3.1 Au NPs experiments in solution

When Au NPs were exposed to ammonium sulphate, a destructive effect was seen immediately. As the amount of ammonium sulphate increased, the nanoparticles showed signs of agglomeration. Initially the changes were quite minor; in fact, at 1% (v/v) the SPR was positively impacted. The peak increased in area but only for this very low concentration. The agglomeration happened gradually after this point until the concentration reached 5% (v/v) where from the SPR we can see a tail forming into the visible range as well as a dramatic shrinking of the peak height. By a concentration of 10% (v/v) the surface plasmon had disappeared entirely and the solution had turned a deep purple-black colour.

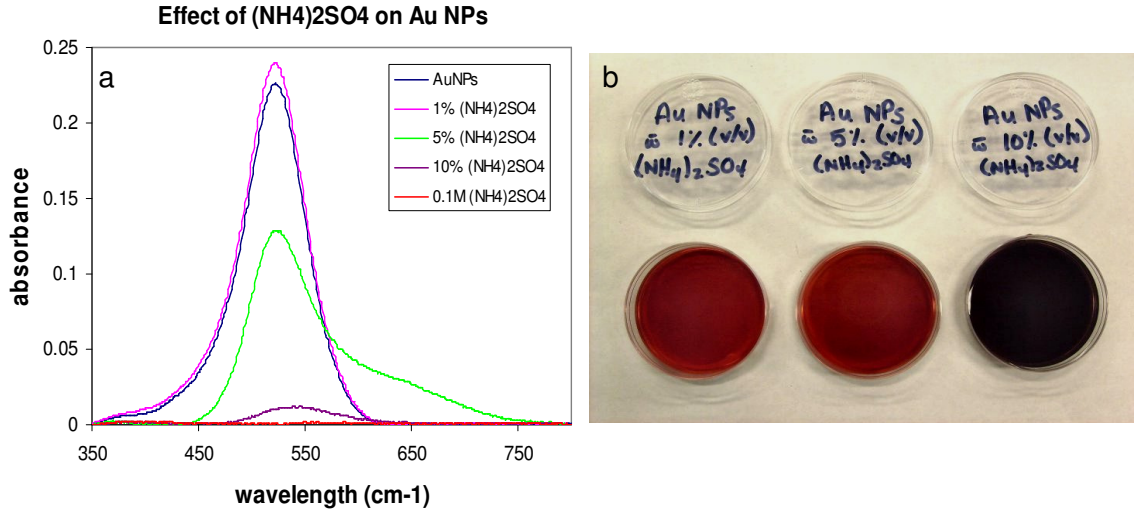

Figure 50: a) SPR spectra of Au NPs exposed to $(NH_4)_2SO_4$. b) Photo taken of Au NPs solutions containing various amounts of $(NH_4)_2SO_4$.

The solutions were also investigated using TEM, where the agglomeration of the particles can be clearly seen. The 1% solution shows only minor agglomeration where the particles can still be clearly distinguished from one another. As the amount of ammonium sulphate increases, one can see more agglomeration until finally there is total agglomeration and the particles can no longer be differentiated from each other.

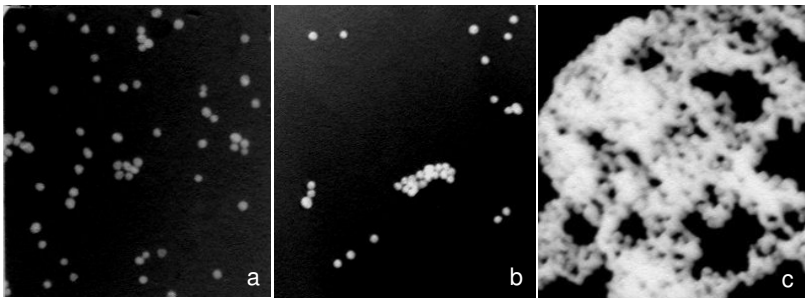

Figure 51: TEM slides of Au NPs exposed to various amounts of $(NH_4)_2SO_4$ a) 1%(v/v) b) 5%(v/v) and c) 10%(v/v).

The results using diethylamine (DEA) instead of ammonium sulphate were quite similar. There was positive interaction initially, which lasted longer in this case. At a concentration of 5% the

SPR had decreased back to that of the blank Au NPs solution. At a 10% concentration the telltale tail into the red direction is apparent.

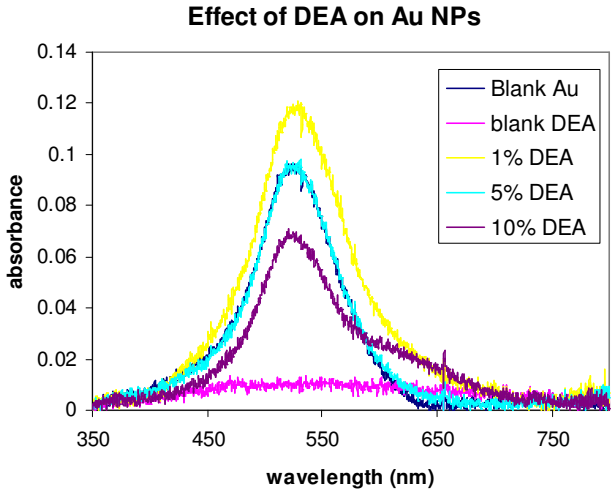

Figure 52: SPR spectra of Au NPs exposed to DEA.

When attempting to investigate the solutions using FTIR the biggest problem was that of solvent absorbance. It is a well known fact that water has many, very large features in its IR spectrum. At the concentrations of both the ammonia species and the nanoparticles used, it was impossible to see their features when compared to the large water features. ATR was attempted instead of transmission IR in the hope that without having to pass through the sample the spectrum of interest would be visible. This was not the case as the water features were still too large. Raman spectroscopy was also attempted as the Raman active features of water have much smaller intensities. It was determined that the concentrations of the species of interest were still too low to obtain a good spectrum.

4.3.2 Surface Treatment

The MPTMS coating was successfully applied and was confirmed using Raman spectroscopy. The first time the slide was soaked in the Au NPs solution it was left for 60 min.

When the Raman spectrum was taken there was no visible change between the coating before and after exposure to gold nanoparticles.

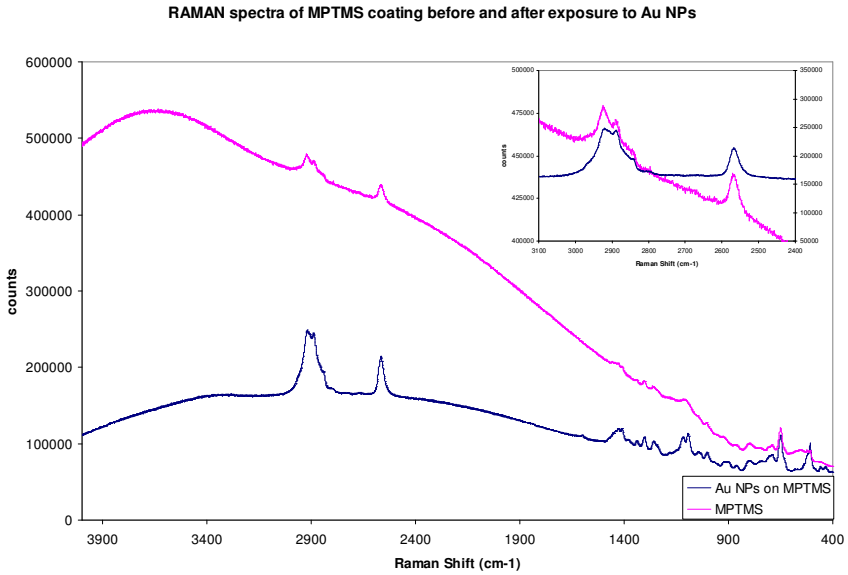

Figure 53: Raman spectra of MPTMS slides before and after 1hr exposure to Au NPs solution.

The exposure time was gradually increased from 60 min to 24 hr and there was no change in the Raman spectra. The only change was that, after being exposed for 24 hr, the slide appeared to have been gold plated, with metallic gold streaks all over the glass surface. It wasn't possible to take the Raman spectrum as the surface fluoresced too much to see the spectrum.

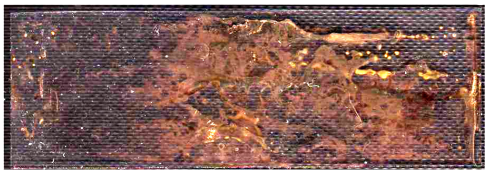

Figure 54: Photo taken of gold 'plating' on MPTMS treated glass slide.

The first modification was to add SDS to the gold solution so that the final concentration of SDS was 0.2 M. The SPR spectra show no shift in the peak and while it has lost intensity, there is no sign of agglomeration. After an hour of exposing the glass

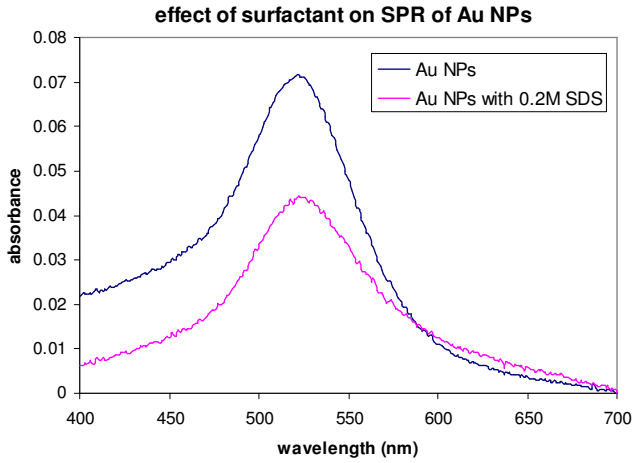

Figure 55: SPR of Au NPs before and after addition of 0.2 M SDS.

slides to the solution, and allowing them to dry, there was no evidence of Au NPs having adhered to the coating. The same result occurred with $SC_{10}SO_3$, a lower concentration was used to keep the particles suspended, but there was still no change in the Raman profile.

4.4 Discussion

4.4.1 Au NPs experiments in solution

Through the addition of ammonium sulphate to the nanoparticle solution, an interaction has been observed, albeit a destructive one. The addition of the ammonium species destabilized the particles and promoted agglomeration. This was confirmed with both UV-visible spectroscopy as well as TEM. Diethylamine was also used to see if a weaker amine species would exhibit the same behaviour, which to some degree it did. It stands to reason that the results of DEA would reflect those of ammonium sulphate with the eventual disappearance of the SPR at high enough concentrations. The next step was to investigate what was happening at the lower concentrations, before destabilization occurred. This was not possible with this method as both FTIR and Raman spectroscopy was unsuccessful at the low concentration of all species. Surface treatment of glass slides with MPTMS was hoped to yield the solution to this problem, as it

would be possible to have a higher concentration of gold particles on the glass surface. It would also eliminate any solvent interference as the slides would be allowed to dry.

4.4.2 Surface Treatment

The glass slides were successfully coated with MPTMS as can be seen in the Raman spectrum as shown in figure 53. The addition of the gold nanoparticles was not successful, again shown in the Raman spectrum by the persistence of the S-H feature at 2561 cm^{-1}. Regardless of how the particles were treated, either by SDS or $SC_{10}SO_3$, it was not possible to get the particles to adsorb. This process had been successfully completed by others using the exact procedure employed here, with the only difference being the method of nanoparticle formation. Laser ablated nanoparticles were used as opposed to the citrate particles made in this work. As laser ablated particles are considered 'clean' due to the absence of dissolved species in the solution, it is possible that this was the cause of lack of success using this method.

References for Chapter 4

1. Grabar KC, Freeman RG, Hommer MB, Natan MJ. Preparation and characterization of au colloid monolayers. Anal Chem 1995 FEB 15;67(4):735-43.

2. Westcott SL, Oldenburg SJ, Lee TR, Halas NJ. Formation and adsorption of clusters of gold nanoparticles onto functionalized silica nanoparticle surfaces. Langmuir 1998 09/01;14(19):5396-401.

3. Liu RQ, Shen W, Zhang JS, Li M. Adsorption and dissociation of ammonia on au(111) surface: A density functional theory study. Appl Surf Sci 2008 JUL 15;254(18):5706-10.

4. Bai T, Cheng XH. Preparation and characterization of 3-mercaptopropyl trimethoxysilane self-assembled monolayers. Journal of University of Science and Technology Beijing 2008 APR;15(2):192-6.

5. Li Y, Wang Y, Tran T, Perkins A. Vibrational spectroscopic studies of (3-mercaptopropyl)trimethoxylsilane sol–gel and its coating. Spectrochimica Acta Part A: Molecular and Biomolecular Spectroscopy 2005 10;61(13-14):3032-7.

6. Thompson WR, Cai M, Ho M, Pemberton JE. Hydrolysis and condensation of self-assembled monolayers of (3-mercaptopropyl)trimethoxysilane on ag and au surfaces. Langmuir 1997 04/01;13(8):2291-302.

Chapter 5
Summary and Future Outlook

The initial aim of this work was to characterize the interactions of metal nanoparticles with small molecules. The most complicated aspect of this was to determine how to get the nanoparticles into a position to both interact with the molecules as well as be available for spectroscopic analysis. All the methods attempted were chosen as they have been used in other situations for just such a purpose.[1-3]

Electrospray ionization was the first method chosen. It was to be used as the source of metal nanoparticles and allow for the small molecules to interact in the gas phase before being frozen in a rare gas matrix for spectroscopic investigation. It was determined, though, that the electrospray apparatus developed for this project had an inherent flaw; the path length was too long to allow the nanoparticles to successfully navigate through to the cold window of the matrix isolation apparatus. The vacuum was insufficiently powerful to compensate and therefore the method was abandoned.

Sol-gel encapsulation was the next approach, and was chosen due to its similarity to the electrospray method. Instead of the metal nanoparticles entering the matrix simultaneously with the small molecules, they would already be present. The sol-gel would be porous enough to allow for the interactions between nanoparticles and the molecules to still occur. The complication associated with the sol-gel method was determined fairly quickly, it was the sol-gel itself. The gels were successfully used for UV/vis spectroscopy, but not for FTIR. It was seen that the gel absorbed all the infrared radiation and thus did not allow any spectrum to be collected. The attempt to use thin films of the nanoparticle containing gels yielded similar results.

In the case of solution chemistry, it was chosen mainly due to its simplicity. The molecules chosen to interact with the nanoparticles were introduced into the nanoparticle solution and given time to react. This method was also abandoned as the solvent features were far greater than any possible feature associated with the nanoparticles. This problem was what led to the idea of increasing the concentration through the use of surface treatments.

This final method would hold the particles on a rigid host as the solution containing the sample was introduced. This would have allowed more interactions to be visible and increase the intensity of the spectroscopic features. This method proved fruitless as it was not possible to get the gold particles to adhere to the surface.

Looking back at the work done, it's possible to determine why each method failed and what could have been done to possibly improve them. In the case of electrospray ionization, the problem was due to the flight distance of metal nanoparticles at atmospheric pressure. For this method to work, the pressure needed to be drastically reduced immediately after the spray chamber. Reducing the distance the particles need to travel would also improve the chances of success. To further aid in the directing of the particles, electrostatic lenses could have been used as well to focus the particle beam.

Sol-gel encapsulation had a fundamental problem. The sol-gel monoliths absorbed all the infrared radiation which prevented any spectroscopic observation of the metal nanoparticle interactions. When a thin film was used to reduce the amount of gel, the concentration of nanoparticles was reduced. This made it impossible to see any features; the peak to noise ratio was far too large to reasonably label any peaks. The only way to try to make this method successful would be to use a different spectroscopic probe, something other than FTIR. If there were a spectroscopic probe to which the sol-gel were transparent or only weakly absorbing, then the gel monoliths could be used which would increase the concentration of nanoparticles.

Solvent absorption was the biggest complication with the solution phase technique used. The concentration of metal nanoparticles, as well as the interacting species, needed to be low in order to keep the nanoparticles suspended. This caused the same problem as with the sol-gel, the support medium dominated the spectrum and no interactions could be observed. The best solution to this problem would be to change either the spectroscopic probe, or the solvent, to reduce the solvents participation. An example of a solvent which could be used with FTIR would be liquid xenon, or another inert gas. Liquid inert gas solvents are spectroscopically transparent from the ultraviolet to the far infrared region.[4] However, there is the question of whether the nanoparticles could be made to be stable in this very unusual environment.

For the surface treatment method, the complication came from the nanoparticles. The nanoparticles could not be bonded to the surface treatment. MPTMS has been shown to bond only weakly with chemically prepared metal nanoparticles. For better results, 3-aminopropyltrimethoxysilane could have been used. The amine demonstrates better bonding to the nanoparticle surface than the thiol functional group.[5]

From all the work completed, the best conclusion of what caused the majority of complications was that of solvent or support interference. If it were possible to remove both the solvent and any need for support there would be nothing present to interfere with the spectral analysis. This leads back to electrospray ionization being the correct approach, as by design, it removes everything from the system except the metal nanoparticle itself.

References for Chapter 5

1. Lenggoro IW, Lee HM, Okuyama K. Nanoparticle assembly on patterned "plus. J Colloid Interface Sci 2006 NOV 1;303(1):124-30.

2. Vreugdenhil AJ, Pilatzke KK, Parnis JM. Characterization of laser ablated gold nanoparticles encapsulated in epoxy amine crosslinked sol-gel materials. J Non Cryst Solids 2006 OCT 1;352(36-37):3879-86.

3. Li Y, Wang Y, Tran T, Perkins A. Vibrational spectroscopic studies of (3-mercaptopropyl)trimethoxylsilane sol–gel and its coating. Spectrochimica Acta Part A: Molecular and Biomolecular Spectroscopy 2005 10;61(13-14):3032-7.

4. Mina-Camilde N, Cedeño DL, Manzanares I. C. FT-IR spectroscopy in liquid xenon solution, ab initio calculations, normal coordinate analysis, and vibrational assignments of meso-2,4-dichloropentane and racemic-2,4-dichloropentane. Spectrochimica Acta Part A: Molecular and Biomolecular Spectroscopy 1998 3;54(3):419-37.

5. Hajduková N, Procházka M, Štěpánek J, Špírková M. Chemically reduced and laser-ablated gold nanoparticles immobilized to silanized glass plates: Preparation, characterization and SERS spectral testing. Colloids Surf Physicochem Eng Aspects 2007 7/5;301(1-3):264-70.